

2



This is to certify that the

dissertation entitled

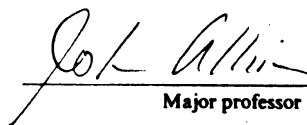
DESIGN AND CHARACTERIZATION OF MIXED TRANSITION
METAL OXIDE THIN FILM GAS SENSORS
DERIVED THROUGH SOL-GEL CHEMISTRY

presented by

Lee W. Hoffman

**has been accepted towards fulfillment
of the requirements for**

M.S. degree in Chemistry


Major professor

Date 3-29-96

LIBRARY

Michigan State University

PLACE IN RETURN BOX to remove this checkout from your record.
TO AVOID FINES return on or before date due.

DATE DUE	DATE DUE	DATE DUE
NOV 02 2000		
MAR 28 2001		
12081		

MSU is An Affirmative Action/Equal Opportunity Institution

c:\circ\d\date.due.pm3-p.1

**DESIGN AND CHARACTERIZATION OF
MIXED TRANSITION METAL OXIDE THIN FILM GAS SENSORS
DERIVED THROUGH SOL-GEL CHEMISTRY**

By

Lee W. Hoffman

A THESIS

**Submitted to
Michigan State University
in partial fulfillment of the requirements
for the degree of**

MASTER OF SCIENCE

Department of Chemistry

1996

ABSTRACT

DESIGN AND CHARACTERIZATION OF MIXED TRANSITION METAL OXIDE THIN FILM GAS SENSORS DERIVED THROUGH SOL-GEL CHEMISTRY

By

Lee W. Hoffman

Several surface and bulk characterization techniques have been used to study the effects that temperature and loading have on the structure of vanadium oxide/titanium oxide thin film conductimetric sensors. This work establishes the crystal structures of the oxides present in the film as well as the oxidation state and the coordination of vanadium.

The mixed oxide thin films were characterized using FTIR, XRD, UV-Vis and XPS. The TiO_2 crystal structure changes from amorphous to anatase to rutile as the annealing temperature is increased. The presence of vanadium lowers temperatures at which phase transformation occurs, even at low loadings. An increased particle size was observed as temperature was increased. XPS results show the change in oxidation state of the surface vanadium ion as temperature as well as a function of loading. A migration of the vanadium species to the surface increased as the annealing temperature increased or the amount of bulk vanadium increased. The coordination and the oxidation state of bulk vanadium ion were obtained through UV-Vis. The TiO_2 band gap remains unchanged as the vanadium loading is increased. However, the TiO_2 band gap is lowered as temperature increases and finally collapses at high temperatures.

To my wife and my son.

ACKNOWLEDGMENTS

When I applied to MSU for graduate studies in chemistry, I planned on furthering my knowledge in this discipline. I had no idea, however, that my knowledge base in many other areas would grow at the same time I as that in chemistry.

As a result, I have many to thank and, as always, first I will thank my family and foremost on this list is my wife, Dawn. She has been a source of steadfast support throughout the time I have been working towards this goal. My son, Stephan, has compromised his desire to have dad there at every moment to “do things” when, instead, much of the time I was absorbed in school. My family patiently waited for this time to come when we can ‘start our new life.’ My parents, too, deserve a “thank-you” for their support in anything I have tried.

Next, I want to thank all the faculty I received help and guidance from at Michigan State University. There are a few in particular that I would like to mention. Dr. Allison helped persuade my decision to attend MSU for graduate studies. When I interact with him, it seems he understands that I am human. That was nice. His assistance these last few months were needed to bring this project to an end, and I really appreciate everything he has done. Also, without Dr. Jeffrey Ledford, the projects described in this thesis would not have been possible. Dr. Ledford was a great source to go to when it seemed like everything I was doing was a waste. I wish he could have been here through the end and I

hope the best for him in the future. I would also like to thank Dr. Paul Hunter. It was a great pleasure teaching under his direction.

The Ledford group deserves many thanks. Paul, you were a great companion, you were there when I needed an ear, sometimes responding with helpful opinions (albeit not always the opinion I would have preferred!). Although our friendship will last, our personal day-to-day interaction will be missed. Mike, you showed me the power of a laugh, especially at myself. Per, Greg and Kathy, your experience with sol-gel chemistry, sensor characteristics, and all the methods used to characterize our films I relied on and are thus an integral part of my research. I want to thank Greg and Per as well for helping me through ‘crisis’ situations in data manipulation and presentation. I would also like to thank many of the current and former Dantus group members. Your support was there when I needed it. And Carl, whom I was mistaken for several times (and vice versa), I am glad our friendship evolved (Stephan and Dawn too).

My final thanks goes out to Jim. I met Jim about a year and a half ago, at the point when I was feeling like my future was pointless. Throughout the time we have known each other, I have been able to put direction back into my life. Like I told him, “I am in the driver’s seat now, and whether I am going to see what is ahead of me or what is behind me is my choice.”

TABLE OF CONTENTS

	Page
List of Tables.....	viii
List of Figures	ix
Chapter 1: Methods to Synthesize and Characterize Thin Film Conductimetric Gas Sensors.....	1
1.1 Introduction	1
1.2 Metal Oxides and Conductimetric Gas Sensing	2
1.2.1 Metal Oxide Semiconductor Surfaces.....	2
1.2.2 Conductivity in Metal Oxides	4
1.2.3 Reactions at Oxide Surfaces.....	8
1.3 An Overview of the Sol-Gel Method	10 -
1.3.1 Transition Metal Sol-Gel Chemistry	11
1.3.2 Metal Carboxylate Thin Film Synthesis Via Carboxylic Acid Complexation	16
1.3.3 Synthesis and Properties of Titanium Oxide Thin Films	18
1.3.4 Synthesis and Properties of Vanadium Pentoxide Gels.....	21
1.4 X-Ray Photoelectron Spectroscopy (XPS)	23
1.5 Ultraviolet-Visible Spectroscopy (UV-Vis).....	26
1.6 X-Ray Diffraction (XRD).....	29
1.7 List of References.....	31
Chapter 2: Effects of Annealing Temperature on the Structure of Vanadium Oxide/Titanium Oxide Thin Films Derived from Metal Carboxylate Sol-Gel Processing.....	36
2.1 Introduction	36
2.2 Experimental	39
2.3 Results and Discussion	42
2.4 Conclusions.....	56
2.5 List of References.....	58

Chapter 3: Effects of Doping Levels on Vanadium Oxide/Titanium Oxide Thin Film Conductimetric Sensors	60
3.1 Introduction	60
3.2 Experimental	62
3.3 Results and Discussion	64
3.4 Conclusions.....	75
3.5 List of References.....	78
Chapter 4: Future Work.....	80
4.1 Sensor measurements	81
4.2 Oxidation Reactions	83
4.3 Reduction Reactions.....	85
4.4 List of References.....	88

List of Tables

Table	Page
Table 2.1. Particle size of TiO ₂ crystals in V/Ti thin films. Calculations made using FWHM of respective XRD feature.	46
Table 2.2. Binding energies of V 2p _{3/2} features as a function of calcination temperature.	51
Table 3.1. Particle size of TiO ₂ (anatase) as determined through line broadening calculations of XRD diffraction patterns.	66
Table 3.2. Measured Band gaps measured for V/Ti films. A film containing TiO ₂ (anatase) crystals is included for reference.	71
Table 3.3. XPS data for films derived from sols containing between 2.5 and 20% V. *Determined from V 2p _{3/2} / Ti 2p _{3/2} intensity ratios.	73

List of Figures

Figure	Page
Figure 1.1. Band model of semiconductor. X is the distance through the semiconducting material and f is the value of the Fermi function. (From Madou, M. J.; Morrison, S. R. <i>Chemical Sensing with Solid State Devices</i> ; Academic Press: San Diego, CA, 1989.).....	3
Figure 1.2. Accumulation and depletion of electrons resulting in a space-charge layer formation. (a) distribution of charges and (b) band scheme near conduction band edge. E_C = conduction band edge; E_F = Fermi level; S = surface states; eV_s = surface potential; x = distance into semiconducting material. (From Cox, P. A. <i>The Electronic Structure and Chemistry of Solids</i> , Oxford University Press, Oxford, 1987.)	5
Figure 1.3. XPS process	24
Figure 2.1. FTIR spectra of (a) V/Ti film annealed at 400°C and (b) Ti film annealed at 400°C.....	43
Figure 2.2. XRD patterns measured for V/Ti films annealed at (a) 300°C, (b) 400°C, (c) 500°C, and (d) 600°C.....	45
Figure 2.3. UV-Vis spectra collected for primarily amorphous thin films containing the following crystalline phases (a) TiO_2 (anatase), (b) TiO_2 (anatase) and TiO_2 (rutile), and (c) V_2O_5	48
Figure 2.4. UV-Vis spectra obtained for V/Ti films annealed at (a) 300°C, (b) 400°C, (c) 500°C, and (d) 600°C.....	50
Figure 2.5. Vanadium $2p_{3/2}$ photoelectron spectra collected for V/Ti films (a) ascast, films annealed at (b) 300°C, (c) 400°C, (d) 500°C, and (e) 600°C and a reference spectra of V_2O_5 (f).....	53
Figure 2.6. Variation in XPS determined V/Ti atomic ratio as a function of annealing temperature	55

Figure 3.1. XRD diffraction patterns obtained for V/Ti atomic ratios of: (a) 0.026, (b) 0.053, (c) 0.111, (d) 0.176, (e) 0.250.....	65
Figure 3.2. UV-Vis spectra for reference films containing (a) TiO ₂ (anatase) or (b) V ₂ O ₅	68
Figure 3.3. UV-Vis spectra for films containing V/Ti atomic ratios of (a) 0.026, (b) 0.053, (c) 0.111, (d) 0.176 and(e) 0.250.	69
Figure 3.4. XPS results showing the effect of vanadium loading on the feature due to V2p _{3/2} . Films were derived from sols with (a) 0.026, (b) 0.053, (c) 0.111, (d) 0.176, and (e) 0.250 V/Ti atomic ratios	72
Figure 3.5. Comparison of surface and bulk V/Ti atomic ratios. Experimental data represented by circles. Spuares represent a plot for equal bulk and surface ratios	74
Figure 4.1. Schematic of sensor array.....	82
Figure 4.2. Cell used to make sensor measurements.	84

Chapter 1

Methods to Synthesize and Characterize Thin Film Conductimetric Gas Sensors

1.1 Introduction

The semiconducting properties of transition metal oxides are well understood, and sensors based on TiO_2 are becoming increasingly popular. Current interest in the chemical sensing properties of these oxides involves issues relative to the monitoring of air pollutants [1]. To date, most sensor studies have focused on single crystals of the metal oxides. Recently, however, the development of sol-gel chemistry has led to new sensor materials based on metal oxide thin films. TiO_2 -based sensors have been studied [2-5] and V/Ti oxide materials have received attention in catalysis studies for the oxidation of hydrocarbons [6,7] and the reduction of NO_x compounds [8-10]. However, sensor studies utilizing the properties of the sol-gel derived V/Ti system have not been investigated. Thus the goal of this work is to characterize vanadium oxide/titanium oxide conductimetric sensors produced via sol-gel chemistry.

Before sensor properties can be studied and/or evaluated, an appropriate system must be developed. In V/Ti catalyst studies, it has been shown that both the amount of vanadium present [10-12] and the temperature at which the catalyst is prepared [13,14] affect the material's structure. It would therefore be appropriate to investigate the affect these two factors have on the structure of sol-gel produced vanadium oxide/titanium oxide thin films. A variety of spectroscopic techniques (XPS, XRD, and UV-Vis) will be used

to characterize both the surface and bulk structures of the films. Prior to describing the results of the study, properties of and reactions occurring on semiconducting metal oxide surfaces will be discussed, along with background on the spectroscopic techniques used for the characterization of these thin films.

1.2 Metal Oxides and Conductimetric Gas Sensing

1.2.1 Metal Oxide Semiconductor Surfaces

A semiconductor is a non-metallic solid that conducts electricity through thermal excitation of electrons across an energy gap. A band model of a semiconductor surface is represented in Figure 1.1. The energy (or band) gap E_G is the energy separating the valence band E_V from the conduction band E_C . Applying this to metal oxides, the valence band is the highest occupied molecular orbital (HOMO) of oxygen while the conduction band is the lowest unoccupied molecular orbital (LUMO) of the metal ion [15]. The Fermi energy E_F represents the energy of the highest filled level. For a semiconductor, E_F is defined to lie in the energy gap between the valence and conduction bands of the electron distribution at the point at which a level has an equal chance of being occupied or empty. The stoichiometric metal oxide has no electron holes in the ground state (contains no defects) [15]. Thus, at any given temperature, the number of electrons in the conduction band of a stoichiometric metal oxide must equal the number of holes in the valence band resulting in the Fermi energy level placed midway between the two bands.

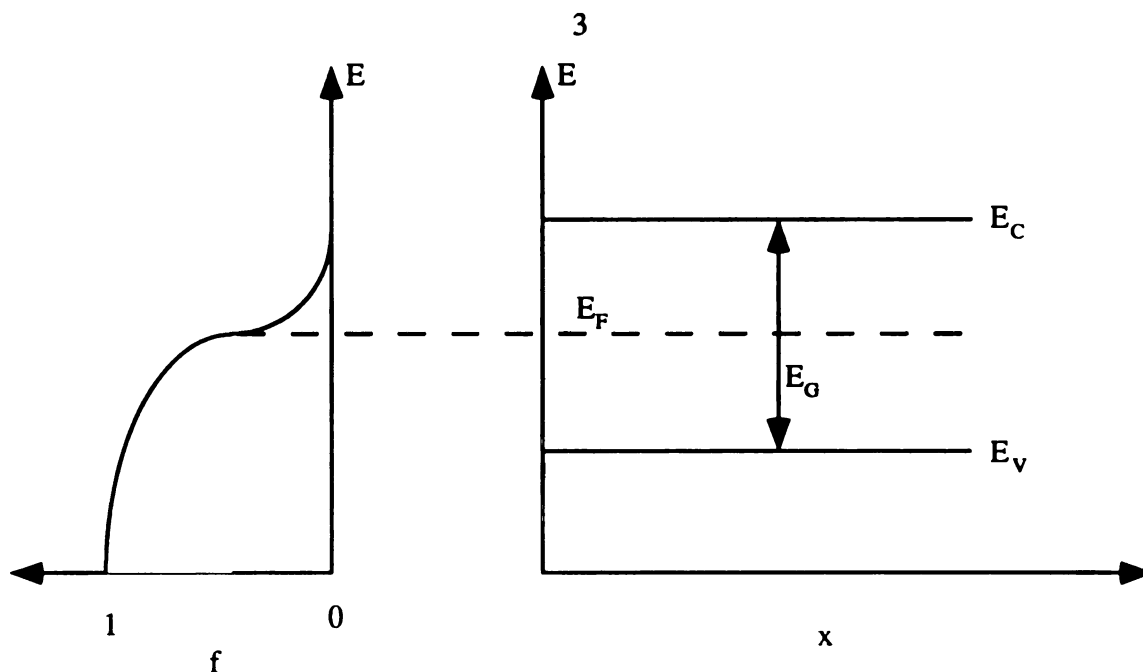


Figure 1.1. Band model of semiconductor. x is the distance through the semiconducting material and f is the value of the Fermi function. (From Madou, M. J.; Morrison, S. R. *Chemical Sensing with Solid State Devices*; Academic Press: San Diego, CA, 1989.)

However, the presence of impurities can affect semiconductors in two ways [15]. First, n-type semiconducting materials result when the number of electrons in the conduction band is greater than the number of holes in the valence band with the Fermi energy level closer to the conduction band. On the other hand, p-type semiconducting materials result when conditions are opposite resulting in the Fermi energy moving closer to the valence band.

Redox properties of transition metal oxides allow these materials to be non-stoichiometric (or contain defects) [16]. Since these oxides can be easily reduced, oxygen atoms may be removed resulting in the reduction of the metal ion. The d electrons of the

metal ion associated with the oxygen vacancies occupy electronic states within the bandgap [16]. Surface defects play an important role in the catalytic processes of semiconducting transition metal oxides. Through thermal treatment, TiO_2 thin films to be used as chemical sensors can be made slightly oxygen deficient (adding electrons to the conduction band), resulting in n-type sensing properties [5].

Surface electronic states, caused by defects (O vacancies) or adsorbed species, modify the band energy near the surface of n-type semiconductors. When the surface of a semiconductor accepts a charge, a space-charge layer of equal but opposite charge is formed. Figure 1.2 shows the influence electron donors or acceptors have on the surface of an n-type semiconductor. The adsorption of electron acceptors such as oxygen removes electrons from the semiconductor. The removal of electrons forms a depletion region in the space-charge layer. The adsorption of electron donors such as hydrogen, on the other hand, will form an accumulation region by donating electrons to the space-charge layer. Thus, as a depletion layer is formed, the removal of electrons decreases the carrier density and the conductance decreases.

1.2.2 Conductivity in Metal Oxides

Metal oxide conductimetric gas sensors utilize changes in conductivity resulting from the chemisorption or reaction of the analyte gas with the oxide surface. Chemisorption of the analyte gas changes the surface potential, the grain boundary potential and contact potential of the oxide surface through electron transfer [17]. The surface of the metal oxide contains a finite number of electron donors (e.g. adsorbed

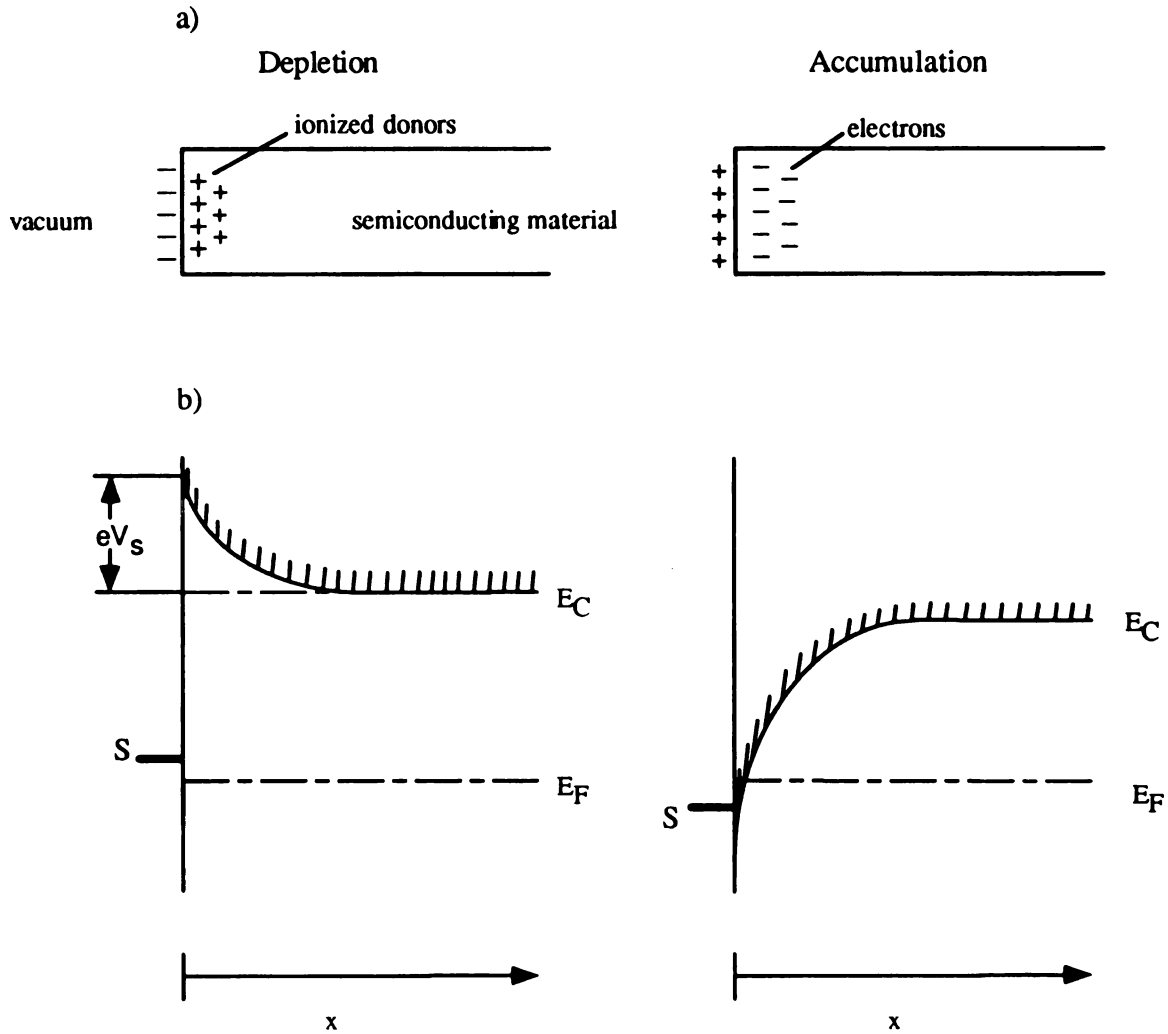


Figure 1.2. Accumulation and depletion of electrons resulting in a space-charge layer formation. (a) distribution of charges and (b) band scheme near conduction band edge. E_C = conduction band edge; E_F = Fermi level; S = surface states; eV_s = surface potential; x = distance into semiconducting material [From Cox, P. A. *The Electronic Structure and Chemistry of Solids*; Oxford University Press; Oxford, 1987].

hydrogen) and/or electron acceptors (e.g. adsorbed oxygen). If we consider a surface saturated with adsorbed oxygen atoms (electron acceptors), a space-charge layer will form near the surface. This layer extends into the interior of the semiconductor through the extraction of electrons from the lattice. Conductivity of this space-charge region is altered by a change in the surface concentration of the ionosorbed oxygen.

The bulk conductivity σ_b of a semiconductor can be expressed as:

$$\sigma_b = n_b q \mu_n + p_b q \mu_p \quad (1.1)$$

where n_b and p_b are the bulk concentrations of the electrons and holes, respectively and q is the electronic charge. (Conductivity is generally expressed as mhos cm^{-1} .) The mobilities of the electrons and holes are represented by μ_n and μ_p , respectively. The mobility of the carrier is its drift velocity per unit electric field and is inversely related to temperature resulting in decreased mobility (lower conductivity) with increased temperature according to the relation below:

$$\mu \propto T^{-3/2} \quad (1.2)$$

Bulk conductance of a semiconducting material is given by:

$$G_b = \sigma_b W t / L \quad (1.3)$$

where W is the width of the film, L is the length, and t is the thickness. The overall conductance of the semiconducting metal oxide sensor is influenced by both surface as well as bulk components G_s and G_b :

$$G = G_b + G_s \quad (1.4)$$

The calculation for the surface conductivity σ_s is different from that of the bulk conductivity in that it does not need to take into account the presence of holes (electron

deficiency) in the oxide lattice. For n-type metal oxide semiconductors such as TiO_2 , changes in surface conductivity $\Delta\sigma$, can be determined using the following equation [18]:

$$\Delta\sigma_s = q\mu_s\Delta n_s \quad (1.6)$$

The number of surface carriers n_s for semiconductors is expected to increase as the temperature increases according to the following relation [15]:

$$n_s \propto \exp(-E_G / 2kT) \quad (1.7)$$

Note that the band gap E_G for most semiconductors is large compared to kT . The predicted Arrhenius-like behavior results in an activation energy equal to one half the band gap of the semiconducting material.

Since we are considering a surface, the conductance is independent of thickness. Surface conductance is therefore expressed in units of mhos or “mhos per square” because the conductance between the sides of a square plate is independent of the size of the square. The change in surface conductance is expressed as:

$$\Delta G_s = \Delta\sigma_s W/L \quad (1.8)$$

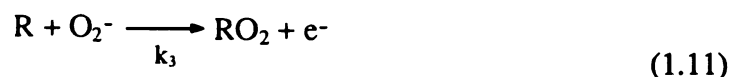
where W is the width of the film and L is the length (the distance between contacts).

There are three generally accepted mechanisms describing the performance of metal oxide sensors based on a barrier to electron transfer: 1) the analyte, reacting with lattice oxygen, will increase the number of defects which in turn increase the number of donor electrons, 2) electrons are injected into the semiconducting surface by adsorption of an electron donating analyte, or 3) oxygen atoms adsorbed on the surface react with the analyte resulting in electrons being injected into the metal oxide surface when the products

desorb [16,19]. Studies of TiO₂ sensors in air have used the third mechanism to describe surface reactions of the sensor with analyte gases [20,21].

1.2.3 Reactions at Oxide Surfaces

Morrison has used a simple model to approximate the sensor response of n-type semiconductors to a reducing analyte [22]. Morrison showed the variation of the surface charge is due to the interaction of oxygen atoms present on the surface with the analyte gas. Several simple reaction steps were postulated:



where the k 's are rate constants, R represents the reducing gas, and e^- is an electron in the conduction band. Only the first equation is considered to be first order since the $[O_2]$ is assumed to be constant. Since gas sensors normally operate at elevated temperatures where O_2^- can be removed from the surface [23], the first equation is reversible. The second reaction is assumed to be irreversible since the reducing gases react readily with O^- . Products of the third and fourth reactions desorb resulting in irreversible reactions. k_3 is considered to be small so it will be omitted from the discussion below.

The total charge on the surface, N_t , can be calculated from the concentration of oxygen species on the oxide surface. We can calculate the concentration of the O_2^- species and the O^- species with the steady state approximations:

$$[O_2^-] = k_1 n_s [O_2] / (k_{-1} + k_2 n_s) \quad (1.13)$$

$$[O^-] = (2k_2 n_s / k_4 [R]) (k_1 n_s [O_2] / \{k_{-1} + k_2 n_s\}) \quad (1.14)$$

where n_s is the electron concentration. The total charge, N_t , can be calculated from these two values using the following equation:

$$N_t = \{k_1 n_s [O_2] / (k_{-1} + k_2 n_s)\} \{1 + 2k_2 n_s / k_4 [R]\} \quad (1.15)$$

Morrison also showed through Schottky's and Boltzmann's relations an exponential increase of n_s with an increase in N_t . Thus, in the equation (1.15), n_s changes significantly with changes in $[R]$ while N_t stays constant. Equation (1.15) may be rewritten in a quadratic from which n_s can be determined:

$$\{2k_1 k_2 [O_2] / k_4 [R]\} n_s^2 + \{k_1 [O_2] - k_2 N_t\} n_s = k_{-1} N_t \quad (1.16)$$

Using this equation, the relationship of n_s as a function of $[R]$ can be used to determine the resistance, ρ , as a function of the partial pressure P_R of the reducing agent:

$$\rho = \alpha / n_s \text{ and } P_R = \gamma [R] \quad (1.17)$$

with α and γ constants. For thin films, the removal of electrons from the surface of the material dominates the material's change in conductivity [24]. The end result is a logarithmic relationship of conductance on $[R]$.

1.3 An Overview of the Sol-Gel Method

Sol-gel chemistry has been used to prepare ceramic materials [25-28]. The materials produced through sol-gel processes may be classified as follows: *sol* - a dispersion of colloidal particles (usually in the range of 1-100 nm) in a liquid, and *gel* - a polymeric chain, whose average length is greater than a micrometer, composed of a rigid network of particles with pores on the submicrometer scale [52].

Advantages the sol-gel process has over conventional methods include easy preparation of multicomponent materials, the use of lower processing temperatures than in traditional ceramic preparations, and the sol and gel rheological properties that allow for fibers, films or composites to be prepared using various techniques such as spinning, dip-coating or impregnation [28]. With sol-gel chemistry, one can control the synthesis from the molecular precursor to the final product, which allows for the fabrication of materials that cannot be obtained through conventional “powder” methods. The properties of sol-gel materials have led to their use in a wide range of applications including the fabrication of optics [27], coatings [26,29], electronic devices [30-32], and sensors [33-36].

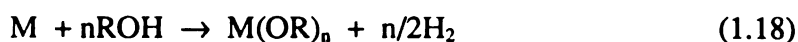
The sol-gel process described here involves the use of transition metal alkoxide precursors to produce metal oxide materials. Transition metals may exist as mixed valences which allows electrons to move from low to high valence states [37]. This leads to oxides of these metals being used as: semiconducting coatings [38], switching devices [39], or electrochromic devices [40]. Since transition metal oxide gels are particle hydrates, they

can exhibit high proton conductivities [41] and some of them behave as inorganic ion exchangers [42].

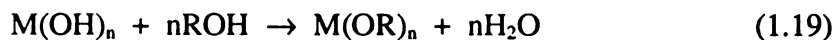
1.3.1 Transition Metal Sol-Gel Chemistry

Mechanisms describing the formation of silicon-based sols and gels have been established [43-47], followed by the development of transition metal sol-gel chemistry; but up till now transitional metal sol-gel chemistry is less understood than silicon sol-gel chemistry. Although many early sol-gel processes involved the use of metal nitrates or halides, the hydrolysis of metal alkoxides has received recent attention. A metal alkoxide may be prepared by using one of three reagents [48]:

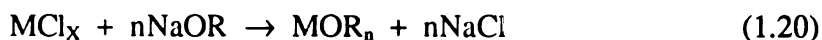
a) a pure metal



b) a metal hydroxide

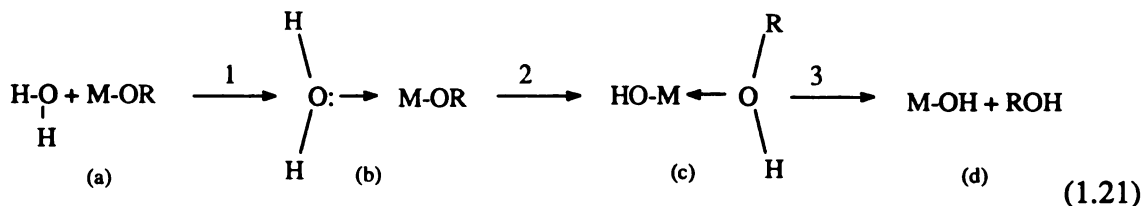


or c) a metal chloride



Metal alkoxides are soluble in a range of organic solvents, most notably in solutions of their parent alcohol. Such solubility is critical to the sol-gel process. Since our synthesis involved the hydrolysis of an alkoxide, it is important that the alkoxide be soluble in a water-miscible solvent such as alcohol.

Most sol-gel preparations involve the hydrolysis of a metal alkoxide followed by condensation and polymerization. Metal hydroxide precipitates are formed from the hydrolysis of metal alkoxides in the presence of water [49,50]. Adding water to the alkoxide causes the formation of a M-OH hydroxo group [28], as represented below:



Steps 1 and 2 show a nucleophilic attack of the metal atom by a water molecule. The electronegative strength of the alkoxo group greatly influences this attack, and will be discussed later. Proton transfer results in the intermediate labeled (c). The final step of this mechanism is the loss of the alcohol to form a metal hydroxide. The rate at which this reaction occurs is referred to as the rate of hydrolysis (k_H).

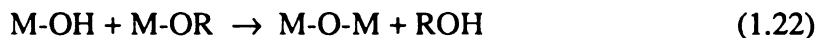
Reactions (1) and (2) occur via S_N2 nucleophilic substitution. The metal center's ability to act as a Lewis acid has a major influence on the substitution reaction. The Lewis acidity of the metal is affected by the coordinative unsaturation and oxidation state of the metal. With increased acidity, proton transfer (to give intermediate c) will occur with a lower activation energy. The electrophilicity of the metal can also affect the k_H of transition metals. More electropositive metals are more susceptible to nucleophilic attack. Electronegative ligands increase k_H by increasing the electrophilicity of the metal [51].

Another way to influence the reactive nature of the metal during hydrolysis is through steric hindrance. Larger alkoxy groups will slow the rate of nucleophilic substitution. Thus, the arrangement of the alkoxide ligand can be used to affect the

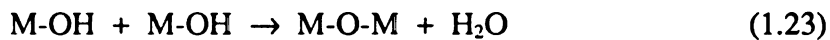
reaction rate during nucleophilic attack. Bulky alkoxide ligands act as better leaving groups and k_H is greater when the alkoxy group is more highly branched. The influence of the ligand on the rate of hydrolysis follows the sequence: primary < secondary < tertiary [28].

The use of non-complexing solvents also influences the rate of hydrolysis. Non-complexing solvents may cause the alkoxide to oligomerize which in turn causes the reduction of k_H due to additional energy that will be required to dissociate the complex [51]. Overall, however, the hydrolysis reaction will be favored when the electrophilic character of the metal is strong and when the leaving ability of the alcohol is high [28,52].

Condensation is initiated by the formation of hydroxyl groups formed during the hydrolysis step, thus it is difficult to separate hydrolysis from condensation. Condensation occurs via three different mechanisms: alcoxolation, oxolation, and ololation [28]. In alcoxolation, a metal oxygen backbone is formed when an alcohol group is removed:



This reaction occurs via an S_N2 mechanism, similar to that of the hydrolysis reaction. Oxolation occurs in a similar manner to reaction 1.22 above, however it involves the removal of a hydroxyl group:



If the coordination of the metal is less than fully satisfied, ololation can occur with alkoxides by the formation of hydroxyl bridges between the metal atoms after the removal of a water or alcohol molecule:



The kinetics of olation are fast when compared to other condensation mechanisms due to the lack of a proton transfer step in the mechanism [28].

For metal alkoxides, the metal's electrophilic character as well as its degree of freedom (amount of coordinative unsaturation) can be used to explain the fact that hydrolysis and condensation occur more rapidly for transition metal alkoxides than for silicon alkoxides. The electrophilic character of some metal alkoxides $\text{M}(\text{OR})_n$ (expressed as the partial charge $\delta(\text{M})$ on the metal atom) [28,53] together with their degree of unsaturation (expressed by the difference $N-n$ where N is the coordination number usually found in the oxide) are as follows:

<u>Alkoxide</u>	<u>$\delta(\text{M})$</u>	<u>$N - n$</u>
$\text{Si}(\text{OPr}^i)_4$	+0.32	0
$\text{Ti}(\text{OPr}^i)_4$	+0.60	2
$\text{Zr}(\text{OPr}^i)_4$	+0.64	3.4
$\text{Ce}(\text{OPr}^i)_4$	+0.75	4

Increasing the electrophilic character and/or increasing the degree of unsaturation will increase the reactivity of a metal center of a metal alkoxide towards nucleophilic substitution.

The hydrolysis and condensation reaction rates for silicon alkoxides are slow and are generally increased using an acid or base catalyst. However, the case for alkoxides with a transition metal center is different - hydrolysis and condensation reactions will often

form precipitates unless they are slowed. The slowing of hydrolysis is most often accomplished through the introduction of complexing ligands that can be bound to the metal center. These ligands slow condensation in two ways: 1) the reactivity of the metal center is lowered by decreasing its electropositive strength and/or steric hindrance and 2) the number of groups available for hydrolysis is lowered. Organic acids and β -diketones are the reagents typically used [51,54-62]. Organic acid ligands are stronger ligands than alkoxides making the metal center more stable with respect to hydrolysis. The role of organic acids in the control of titanium alkoxide hydrolysis has received much attention in the literature [56-58,62-66].

Condensation can be controlled through modification of the water/metal alkoxide ratio. Through determination of the weight percent of TiO_2 in the polymer, Yoldas *et al.* [67] have shown that modifying the water ratio,

$$h = \frac{[\text{H}_2\text{O}]}{[\text{M}(\text{OR})_z]} \quad (1.25)$$

will modify the structure of the final product. Yoldas [68] also found that an increased oxide content of the hydrolysis product is observed when the water ratio is increased. Livage [28] used this finding to derive the following three domains: When $h < 1$, alcoxolation and oxolation condensation reactions occur primarily. As a result, alkoxy bridges are formed and gelation cannot occur since there is no excess water. When $1 \leq h \leq z$ (z is the oxidation state of the metal), competition between alcoxolation and oxolation results and chain polymers are formed. Alcoxolation is favored for $h < 2$; but when h approaches z , hydrolysis may not go to completion and oxolation may result. When $h > z$,

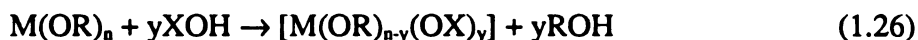
precipitation occurs quickly and condensation occurs via olation as contrasted to oxolation resulting in polymers formed by crosslinking [28].

From the microstructural point of view, silicate sol-gel chemistry differs from non-silicate sol-gel chemistry in three ways: (1) due to the d-orbital configuration of transition metal alkoxide compounds, ligand field stabilization can be used to obtain varied structures [67]; (2) the structure of the polymer obtained can vary widely since the coordination numbers of transition metals range from 2-8; and (3) since metal alkoxides are more electropositive, they are often oligomeric. The size of the metal as well as the size and nature of the alkoxide ligand will determine the steric demands on the metal alkoxide. These demands will influence the extent to which the metal alkoxide will form oligomers [48]. The oligomers are then used as building blocks in the resulting polymer through suitable chemical modification.

1.3.2 Metal Carboxylate Thin Film Synthesis Via Carboxylic Acid Complexation

It is essential to control k_H when producing transition metal oxide thin films via the sol-gel process [28,49,51,69,70]. This control allows the materials to be made from alkoxide precursors without forming precipitates. The extent of hydrolysis is lowered by replacing the more reactive alkoxide ligands with chemical additives such as β -diketones [71], organic acids [56,61,72], and glycols [48].

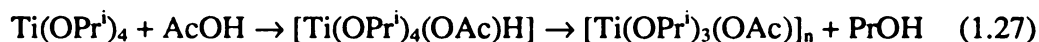
Carboxylic acids can act both as chelating ligands as well as oxygen donors (especially towards oxophilic metals). The alkoxide group is replaced by a carboxylic acid as shown in the reaction below [28]:



Carboxylate ligands behave as terminating reagents on the metal. There are four possible arrangements the carboxylate ligand could form with the metal: ionic, unidentate and bidentate bridging, or chelating [73]. The number and arrangement of carboxylate ligands accepted by a metal center will depend on the metal's size, charge, and number of available sites.

After a carboxylic acid has been added to an alkoxide precursor, addition of water initiates hydrolysis and condensation. Hydrolysis is slowed as the carboxylate ligand is a poorer leaving group than the alkoxide[64]. The increased size of the ligand will slow the rate of hydrolysis even further by inhibiting attack through increased steric hindrance [74].

The chemical control of hydrolysis and condensation of metal alkoxide-carboxylate chemistry can be demonstrated in the reaction of titanium isopropoxide with acetic acid. Partial charge calculations show that the HOAc group in the intermediate, shown below, to be negatively charged ($\delta_{AcOH} = -0.7$) while the Pr^iOH group is positively charged ($\delta_{Pr^iOH} = +0.1$). With the coordination of Ti not being satisfied and a positive partial charge on Ti, AcOH displaces Pr^iOH through nucleophilic substitution in the following condensation reaction:



the acetate groups form bidentate bridging ligands resulting in an oligomeric species where Ti expands its coordination from four to six [74]. Hydrolysis of the oligomeric species leads to:



The continuity of thin films has been studied by Berglund, *et al.* [63,64,75]. They showed that careful choice of appropriate acid:metal (R_a) and water:metal (R_w) ratios is necessary for producing a good film. Their work resulted in the formation of thin and transparent continuous films that show controlled shrinkage and were not brittle.

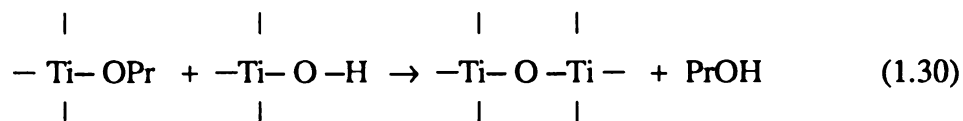
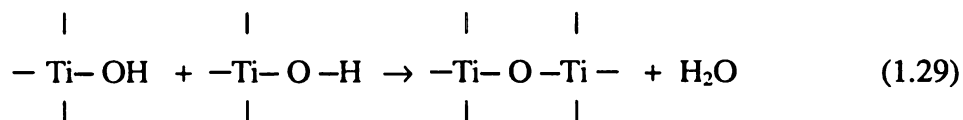
1.3.3 Synthesis and Properties of Titanium Oxide Thin Films

Titanium dioxide plays a significant role in sensing materials. TiO_2 -based materials exhibit surface adsorption properties that are sensitive to water vapor and other gases [76,77]. The hydrolysis of titanium isopropoxide occurs rapidly and can be carried out completely before the start of condensation if the conditions are acidic. These conditions lead to transparent monolithic gels which can be used to produce crystalline TiO_2 in the anatase or rutile form [67]. (Anatase and rutile are two naturally occurring crystal modifications of TiO_2 - rutile the most common.) Under basic conditions, carboxylate ligands remain attached to the Ti atom causing hydrolysis and condensation to occur simultaneously. As a result, crystallization is prevented and amorphous powders are obtained where the morphology depends on the pH [74].

Titanium alkoxide precursors have been used in many recent studies involving sol and gel formation. $\text{Ti}(\text{OR})_4$ (where $R = \text{Bu}^n, \text{Bu}^s, \text{Et}, \text{Pr}^i, \text{Pr}^n$) has been used with

inorganic acid catalysts (HCl, HNO₃) to produce monolithic TiO₂ gels [67,78]. The hydrolysis ratio h of these systems was controlled such that $1 < h < 4$. TiO₂ gels were obtained through control of the hydrolysis ratio, while sols of these systems were produced through use of a proper acid:alkoxide ratio [67,79-81].

Severin *et al.* [66] have also described the production of TiO₂ thin films via the sol-gel process. The titanium isopropoxide precursor was modified by mixing it with valeric acid followed by the addition of water. Sols produced from the valeric acid modified alkoxides have better adhesion to glass and greater integrity than sols produced using other carboxylic acids [63]. Following the reaction scheme previously described, a complexation and hydrolysis reaction of Ti(OPrⁱ)₄ results in the formation of a metal oxide backbone:



An oligomeric structure where the Ti coordination from 4 to 6 has been observed through chemical modification of the alkoxide precursor with organic acids [56,66,72]. Both bidentate and bridging carboxylate ligands have been observed [56,66].

Heat treatment of valeric acid modified titanium alkoxide thin films at moderate temperatures (250°C - 600°C) removes the carboxylate ligands leading to an increase in the titanium-oxygen backbone concentration [82]. At higher temperatures, crystalline

anatase (600°C) and rutile (800°C) regions appear in the film. In all cases the film is primarily amorphous. Crystalline phases in TiO₂ thin films prepared through other sol gel techniques have also been reported [83]. These studies showed that doping lowers the temperature needed for phase transformation of TiO₂.

Although thin TiO₂ films have not been utilized in conductimetric sensing, there has been extensive sensor research on employing TiO₂ both as a single crystal and in polycrystalline forms. The kinetics and thermodynamics of the reaction of the TiO₂ surface with analyte gases are influenced by surface defects [84]. These defects significantly affect the charge transfer between the semiconductor and electrolyte [85]. Dopants in the form of tri- or pentavalent cations create defects (oxygen vacancies) into the TiO₂ lattice [5].

TiO₂ sensors have been used to monitor the combustion of fuel in engines through the detection of oxygen [2-5]. Bulk defects of these sensors are thermodynamically controlled [5] and can be used at high temperatures to determine the oxygen concentration over a wide range of partial pressures. Tri- and pentavalent cations are used to control the sensitivity and conductivity of the sensor. The response of Pt-doped TiO₂ sensors prepared at low temperatures has been attributed to Schottky diode characteristics between the metal and the semiconducting material [2].

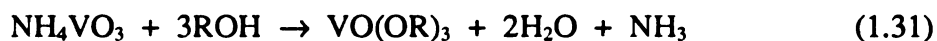
TiO₂-based sensors for the detection of nitrogen-containing compounds have also been studied [86,87]. The reaction mechanism of these sensors varies with the dopant added. For MoO₃/TiO₂ sensors, sensor response to ammonia has been attributed to oxidation involving lattice oxygen [86]. Boccuzzi *et al.* [87] have shown that for TiO₂ or

Ru/TiO₂, the adsorption site for nitrogen containing compounds was the Lewis acid site with Ti⁴⁺.

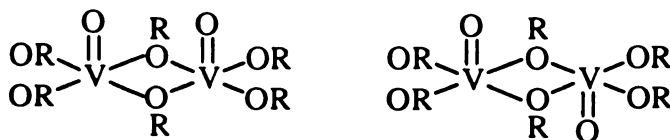
1.3.4 Synthesis and Properties of Vanadium Pentoxide Gels

The catalytic, electronic, and ionic properties of V₂O₅ [88-91] are interesting from the standpoint of chemical sensing. The basicity of bridging oxygens as well as the strong Lewis acidity associated with V⁵⁺ provides reaction sites for the oxidation of hydrocarbons, NO_x reduction, and dehydration of alcohols [88,92,93].

A common way to prepare vanadium alkoxides involves the heating of an ammonium metavanadate mixture under reflux in benzene [94]:



where R = OPrⁿ, OAm^l. Monomers or dimers can be formed depending on the size of the alkoxide group. The structures of vanadium alkoxides was studied by Sanchez *et al.* [95]. Large, bulky groups such as OAm^l prevent coordination expansion of the vanadium atom and produce a monomeric structure via alkoxy bridging. VO(OPrⁿ) forms a dimeric species via edge sharing of alkoxy bridges to give:



The high electrophilicity of the vanadium atom causes the vanadium alkoxides to be very reactive towards hydrolysis. Alkoxy groups become harder to remove as hydrolysis proceeds, thus a large amount of water is needed to completely remove all

groups [96]. A large water to metal ratio produces a highly cross-linked oxide network [91] that has a structure close to that of the crystalline oxide [96]. However, not all alkoxy groups are removed when hydrolysis ratios are low ($h \leq 3$). In this case, a gel is formed which can best be called an alkoxo oxide $[V_2O_{5-x}(OR)_x]_n$ [95]. Oligomers are obtained from vanadium alkoxides reacted with low hydrolysis ratios ($h < 1$) [91].

Since V^{5+} is a strong oxidizing agent, V_2O_5 gels always contain reduced V^{4+} ions [97]. This results in a mixed valence compound whose semiconducting properties arise from electron hopping between the two valence states. Methods of further reduction of vanadium pentoxide gels include exposure to air and dehydration as well as reaction of the gel with the solvent [91]. Along with affecting the hydrolysis reaction, the size of the alkoxide group attached to vanadium also affects the magnitude of reduction. Only 1% of the V^{5+} centers were reduced to V^{4+} when $VO(OAm^t)_3$ was used as a precursor while 10-15% of V^{5+} was reduced when $(OPr^n)_3$ was used [95].

Much of the work surrounding vanadium pentoxide xerogels (a gel formed when the liquid is removed at ambient pressure by thermal evaporation causing shrinkage) has involved the study of its electronic conducting properties and their dependence on temperature and humidity [91]. Vanadium's interesting catalytic chemistry along with the newer opportunities provided by sol-gel chemistry have led to an increased interest in using vanadium pentoxide xerogels for chemical sensors.

There has been a wide use of V_2O_5 in conductimetric sensing. Inubishi *et al.* [98] utilized the influence of relative humidity on the proton transfer conductivity of the oxide to construct a humidity sensor. By doping the vanadium xerogel with various metal

oxides, the structure of the gel was changed. Inubishi reported that changes in structure resulted in a change of the electronic structure, and sensor response was attributed to these changes in electronic structure. Glezer and Lev [99] used amperometric glucose sensors to examine the proton conducting properties of V_2O_5 , while polymer composite sensors were studied by Rushau *et al* [100]. Utilizing both the catalytic activity and electronic properties of vanadium oxide, high temperature conductimetric gas sensors have been developed for analytes such as hydrocarbons, alcohols, NO, and NO_2 [101, 102].

1.4 X-Ray Photoelectron Spectroscopy (XPS)

Photoelectron spectroscopy provides quantitative and qualitative information about the surface structure and composition of a material using the photoemission of electrons [103-105]. X-ray photoelectron spectroscopy (XPS) is one of the most powerful surface sensitive techniques for the study of electronic structure of filled levels of surface atoms. XPS can probe both the valence and core level electrons of a material.

Light consists of photons with energies given by the expression:

$$E = h\nu \quad (1.32)$$

and solids contain a frequency threshold below which light cannot eject electrons from a particular metallic surface. The minimum energy required to remove an electron from the metal surface, $e\phi$, can be calculated from this threshold frequency, ν_c :

$$e\phi = h\nu_c \quad (1.33)$$

where ϕ denotes the work-function of the material and e is the magnitude of the electron charge.

Above the threshold frequency, the emitted electrons will have a maximum kinetic energy that corresponds to the difference between the incident photon and the work function. For the maximum kinetic energy the emitted electrons must be at the Fermi level, that is, the highest lying occupied electronic state of the metal. Photons emitted below the maximum kinetic energy signify electrons emitted from a level having a binding energy E_B . Therefore, the kinetic energy of the ejected electron is the difference between the energy of the incident photon and the binding energy of the core electron (Figure 1.3), taking into consideration the work-function $e\psi$ of the spectrometer:

$$E_k = h\nu - E_B - e\psi \quad (1.34)$$

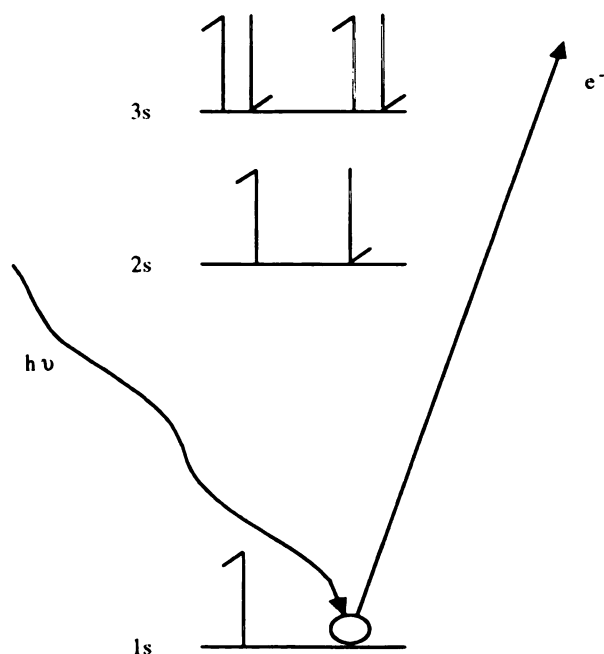


Figure 1.3. XPS process.

Photoelectron spectroscopy thus allows the determination of the relative population of electronic states of atoms.

Binding energies of electrons in molecules will depend on the environment. An increase in the electronegativity of the ligands about a central atom causes a displacement of the valence electrons from the atom towards its ligands. The core electrons therefore encounter a stronger attraction since fewer electrons surround the nucleus resulting in an increase in binding energy [105]. Two balancing factors - the oxidation state of the atom and the Madelung potential of the lattice - cause a chemical shift that changes the binding energy of the core electrons. The subsequent chemical shift of the core electrons from the atomic binding energy can reveal information about the binding environment of an atom.

The XPS signal intensity varies for each particular element and has been defined as follows [106]:

$$I_i = I_0 \eta_i \sigma D(\epsilon_i) \lambda(\epsilon_i) \quad (1.35)$$

where I_0 is the X-ray flux, η_i is the number density of atoms i , σ is the photoexcitation probability of electrons corresponding to a particular atomic orbital of species i , $D(\epsilon_i)$ is the fraction of electrons detected by the analyzer, and $\lambda(\epsilon_i)$ is the mean free path of the emitted electron.

In order to obtain quantitative information about a material, relative intensities of the XPS features are compared. The following relationship has been derived [107]:

$$\frac{\eta_1}{\eta_2} = \frac{I_1}{I_2} \frac{\sigma_2 D(\epsilon_2) \lambda_T(\epsilon_2)}{\sigma_1 D(\epsilon_1) \lambda_T(\epsilon_1)} \quad (1.36)$$

where η_1/η_2 is the relative concentration of species 1 and 2 with I_1/I_2 representing the relative intensities. The remaining values of the equation are assumed to be constant and contribute to a “sensitivity factor” particular to the material being studied. These sensitivity factors can be derived theoretically using previously determined values for σ [106] and $\lambda(\epsilon)$ [107] with $D(\epsilon_2)/D(\epsilon_1)$ measured experimentally or deduced from design specifications. Values for sensitivity factors may also be derived empirically [103]. To derive these empirical values, XPS intensities for a known material (say pure TiO_2) are obtained and used to calculate I_1/I_2 . From this value, along with η_1/η_2 calculated from the known stoichiometry, sensitivity factors can then be calculated.

1.5 Ultraviolet-Visible Spectroscopy (UV-Vis)

UV-Vis measurements involve the partial absorption of electromagnetic radiation [108,109], causing a decrease in the transmitted power of electromagnetic radiation through a sample. When absorption of a photon occurs, the energy of this photon is equal to the energy difference between the ground state and one of the excited energy levels of the absorbing species. Since this difference in energy is specific for a given species, absorption spectra are useful as qualitative and quantitative measures of a substance.

During absorption, a species M is modified by the absorption of a photon, to an excited state M^* as shown below:



In a short time (on the order of nanoseconds) the excited species may lose this energy, most commonly in the form of heat:



Relaxation can also occur through photochemical decomposition of M^* to other products or by fluorescent or phosphorescent radiation emission. The lifetime of the excited species is generally small and its concentration is therefore negligible.

For inorganic molecules, the radiation absorbed may be the result of transitions between filled and unfilled d orbitals. There are several factors that will affect the differences of energy between these orbitals : 1) the position of the element in the periodic table, 2) its oxidation state, and 3) the nature of the ligand bonded to the element [110]. The environment surrounding the transition metal strongly influences the photon absorption.

The electronic transitions involved with the absorption process occur in the partially filled d orbitals of transition metals. Electrostatic repulsion between the electron pairs of donors and the d orbital of the metal ion results in the splitting of d -orbital energies. Energy transferred to an electron in a d orbital of lower energy to an orbital of higher energy can be caused by the absorption of a photon.

There are five representations for the electron-density distributions or “orbitals” of d -electrons: d_{xy} , d_{xz} , d_{yz} , $d_{x^2-y^2}$, and d_{z^2} . The first three are formed between the spatial axes x , y , and z , and consequently, the d_{xy} , d_{xz} , and d_{yz} orbitals have their maximum densities between the axes. The other two representations have their electron densities directed on the axes.

For a molecule in an octahedral formation, the π donor atoms will exert a repulsion on the orbitals increasing the energy of these orbitals causing them to become destabilized. The repulsion for the d_{xy} , d_{xz} , and d_{yz} orbitals will be equal considering their axes do not match with the bonding axes and differ only in orientation. There is a greater effect, however, on the d_{z^2} and $d_{x^2-y^2}$ since their charge densities lie along the axes, resulting in a smaller increase in energy. When considering a tetrahedral structure of atoms around the central metal ion, similar arguments to those made for the octahedral structure can be made. However, under tetrahedral conditions, the relative increase of energies for the two groups (d_{xy} , d_{xz} , and d_{yz} or d_{z^2} and $d_{x^2-y^2}$) is reversed.

The visible spectrum can also be used to measure the band gap in semiconducting materials [111]. The electrons in a semiconductor occupy allowed energy bands resulting from the interactions of atomic energy levels. As stated earlier, the highest occupied band is referred to as the valence band (E_V), the lowest unoccupied is referred to as the conduction band (E_C), and the energy between these two is the energy (band) gap (E_G). Absorption of incident radiant energy can excite the electrons from the valence to conduction band. The minimum amount of energy needed for absorption to occur indicates the band gap energy of the semiconducting material. Thus, when the energy of a quantum ($h\nu$) equals E_G , absorption of light will occur:

$$E_G = \frac{h\nu}{\lambda_G} \quad (1.39)$$

When the wavelength (λ_G) is measured in nm, the calculated band gap is usually measured in units of eV.

1.6 X-Ray Diffraction (XRD)

Since X-rays have wavelengths on the order of Angstroms they are well suited to study the structure of materials [108]. XRD is a bulk characterization technique and can be used for particle size estimations, determination of bulk phases, and quantification of the extent of bulk transformations.

X-ray photons are elastically scattered by atoms in a periodic lattice in the material being studied. The lattice spacing is derived from the diffraction of X-rays by crystal planes using the Bragg equation [112]:

$$n\lambda = 2d \sin(\theta) ; n = 1, 2, \dots \quad (1.40)$$

where λ is the wavelength of the X-rays, d is the distance between two lattice planes, θ is the angle between the incoming X-rays and the normal to the reflecting lattice plane, and n is called the order of reflection. The X-ray photon will only reach the detector when equation (1.40) is satisfied. At all other instances, destructive interference prevents the X-ray photons from being detected. Since the angle of the incoming X-rays will be the same as the reflection angle of the X-rays with respect to the normal to the lattice plane, the angle measured by the diffractometer is 2θ . By measuring the angle, 2θ , at which the detected X-rays are scattered, the lattice spacing, d , of the crystal can then be calculated. From this spacing, the corresponding compound or crystallographic phase of a particular compound can then be determined.

XRD data can also provide information on the particle sizes in materials being studied. Poorly crystallized materials containing large particles show broad features with

peaks narrowing as a more perfect crystal is obtained. Particle sizes can be determined using full width half maximum (FWHM) measurements with Scherrer's equation [113]:

$$L = \frac{K\lambda}{\beta \cos\theta} \quad (1.41)$$

where λ is the X-ray wavelength, β is the peak width, θ is the angle between the X-ray and the normal to the surface, and K is a constant related to the crystalline shape and the way L and β are defined. K is assumed to be ~ 0.9 for the Scherrer equation [114].

Particle sizes determined through the line-broadening technique should be used for relative measures of average particle size. XRD line widths are influenced by the distribution of particles, internal strain, and instrumental factors leading to line broadening. Thus absolute particle sizes cannot be determined using line width measurements [115].

X-ray diffraction provides important information about the influence mixing has on the crystalline phase of vanadium and/or titanium in sol-gel derived thin films after being annealed. Since XRD does not detect amorphous species, the point at which crystalline species are formed (if they are formed), as well as the occurrence of phase changes within the crystal can be determined.

1.7 List of References

1. Meixner, H.; Gerblinger, J.; Fleischer, M. *Sens. Act.* **1993** 15-16, 45.
2. Xu, Y.; Yao, K.; Zhou, X.; Cao, Q. *Sensors and Actuators*, **1993**, B13-14, 103.
3. Wu, M. T.; Yao, X.; Yuan, Z. H.; Sun, H. T.; Wu, W. C.; Chen, Q. H.; Xu, G. Y. *Sensors and Actuators*, **1993**, B13-14, 491.
4. Hasegawa, S.; Sasaki, Y. Matsuhara, S. *Sensors and Actuators*, **1993**, B13-14, 509.
5. Kirner, U., Schierbaum, K. D.; Göpel, W.; Liebold, B.; Nicoloso, N.; Weppner, W.; Fischer, D.; Chu, W. F. *Sens. Act.*, **1990**, B1, 103.
6. Rao, C. N. R.; Raju, A. R.; and Vijayamohanan, K., Gas-sensor Materials in *New Materials*, S.K. Joshi, C.N.R. Rao, R Rsruta and S. Nagakura (eds.)), New Delhi, India, 1992, pp. 1-37.
7. Martin, C.; Rives, V.; Sanchez-Escribano, V.; Busca, G.; Lorenselli, V.; and Ramis, G., *Surf. Sci.* **1991** 251/252, 825.
8. Tufano, V. and Turco, M., *Appl. Catal.* **1993** B2, 9.
9. Turco, M.; Lisi, L.; Pirone, R.; *Appl. Catal.* **1994** B2, 133.
10. Went, G. T.; Leu, L.-J., Rosin, R. R.; and Bell, Alexis T.; *J. Catal.* **1992** 134, 492.
11. Busca, G.; Centi, G.; Marchetti, L.; Trifiro, F. *Langmuir* **1986** 2, 568.
12. Nickl, J.; Schlögl, R.; Baiker, A.; Knözinger, H.; Ertl, G. *Catal. Ltr.* **1989** 3, 379.
13. Vejux, A. and Courtine, P.J. *Solid State Chem.* **1978** 23, 93.
14. Saleh, R.Y.; Wachs, I.E.; Chan, S.S.; Chersich, C.C. *J. Catal.* **1986** 98, 102.
15. Cox, P. A. *The Electronic Structure and Chemistry of Solids*, Oxford University Press: Oxford, 1987.
16. Madou, M. J.; Morrison, S R. *Chemical Sensing with Solid State Devices*; Academic Press: San Diego, CA, 1989.
17. Geistlinger, H. *Sens. Act.* **1993** 17, 47.
18. Janata, J. *Principles of Chemical Sensors*, Plenum Press, New York, 1989.
19. Morrison, S. R. *Sens. Act.* **1982** 2, 329. Advani, G. N.; Nanis, L. *Sens. Act.* **1982** 2, 201.
20. Chang, S. C. in *Chemical Sensors*, Analytical Chem. Symposia Series 17; Elsevier, Amsterdam, 1983 (Fukuoka Conference); eds. T. Seiyama, K. Fueki, J. Shiokawa, S. Suzuki, p.78.
21. Thorton, E. W.; Harrison, P. G. *J. Chem. Soc. Faraday Trans. I* **1975**, 71, 461.
22. Morrison, S. R. *Sens. Act.* **1987** 11, 283.
23. Morrison, S. R. *Surf. Sci.* **1971** 27, 586.
24. Cooper, R. B.; Advani, G. N.; Jordan, A. G. *J. Electron. Mater.* **1981** 10, 455.
25. Reuter, H. *Adv. Mater.* **1991** 3, 569.
26. Reuter, H. *Adv. Mater.* **1991** 3, 258.
27. Ulrich, D. R. *J. Non Cryst. Sol.* **1988** 100, 174.
28. Livage, J.; Henry, M.; Sanchez, C. *Prog. Solid St. Chem.* **1988** 18, 259.
29. Kozhukharov, V.; Trapalis, CH.; Samuneva, B.; Kirilova, E. *J. Mater. Sci. Lett.* **1992** 11, 1206.

30. Grammatico, J. P.; Porto Lopez, J. M. *J. Mater. Sci. Mater. Elect.* **1992**, *3*, 82.
31. Mosset, A.; Gautier-Luneau, I.; Galy, J.; Strehlow, P.; Schmidt, H. *J. Non-Cryst. Solids* **1988**, *100*, 339.
32. Greismar, P.; Papin, G.; Sanchez, C.; Livage, J. *J. Mater. Sci. Lett.* **1990**, 1288.
33. Inubishi, A.; Masuda, S.; Okubo, M.; Matsumoto, A.; Sadamura, H.; Suzuki, K. in *High Tech Ceramics*, P. Vincenzini, Ed., Elsevier Science Publishers, Amsterdam, 1987, 217.
34. Yoshimura, N.; Sato, S.; Itoi, M.; Taguchi, H. *Sozai Busseigaku Zasshi* **1990**, *3*, 47.
35. Levy, D. *J. Non Cryst. Solids* **1992**, *147&148*, 508.
36. Lev, O. *Analysis* **1992**, *20*, 543.
37. Austin, I.G.; Mott, N.F. *Adv. Phys.*, **1969**, *18*, 41.
38. Bullo, J.; Gallais, O.; Gauthier, M.; Livage, J. *Appl. Phys. Lett.*, **1980**, *36*, 986.
39. Bullo, J.; Gallais, O.; Gauthier, M.; Livage, J. *Phys. Stat. Sol. A*, **1982**, *71*, K1.
40. Chemseddine, A.; Morineau, R.; Livage, J. *Solid State Ionics*, **1983**, *9-10*, 357.
41. Barboux, P.; Baffier, N.; Morineau, R.; Livage, J. *Solid State Ionics*, **1983**, *9-10*, 1073.
42. Aldebert, P.; Baffier, N.; Legendre, J.J.; Livage, J. *Rev. Chim. Min.*, **1982**, *19*, 485.
43. Brinker, C.J.; Clark, D.E.; Ulrich, D.R., Eds.; *Mat. Res. Soc. Symp. Proc.* 32, Materials Research Society, Pittsburgh, 1984.
44. Brinker, C.J.; Clark, D.E.; Ulrich, D.R., Eds.; *Mat. Res. Soc. Symp. Proc.* 73, Materials Research Society, Pittsburgh, 1986.
45. Brinker, C.J.; Clark, D.E.; Ulrich, D.R., Eds.; *Mat. Res. Soc. Symp. Proc.* 121, Materials Research Society, Pittsburgh, 1988.
46. Zelinski, B.J.J.; Brinker, C.J.; Clark, D.E.; Ulrich, D.R., Eds.; *Mat. Res. Soc. Symp. Proc.* 180, Materials Research Society, Pittsburgh, 1990.
47. Hampden-Smith, M.J.; Klemperer, W.G.; Brinker, C.J., Eds.; *Mat. Res. Soc. Symp. Proc.* 271, Materials Research Society, Pittsburgh, 1992.
48. Bradley, D.C.; Mehrotra, R.C.; Gaur, D.P. *Metal Alkoxides*, Academic Press, London, 1978.
49. Zheng, H.; Colby, M.W.; Mackenzie, J.D. *Mater. Res. Soc. Symp. Proc.* **1988**, *121*, 537.
50. Guglielmi, M.; Carturan, G. *J. Non-Cryst. Solids* **1988**, *100*, 16.
51. Sanchez, C.; Livage, J.; Henry, M.; Babonneau, F. *J. Non-Cryst. Solids* **1988**, *100*, 65.
52. Hench, L. L.; West, J. K. *Chem. Rev.* **1990**, *90*, 33.
53. Livage, J.; Henry, M. in *Ultrastructure Processing of Advanced Ceramics*, Mackenzie, J.D.; Ulrich, D.R., Eds., Wiley, New York, 1988, 183.
54. Mehrotra, R.C.; Gaur, D.P.; Bohra, R. *Metal β -diketonates and Allied Derivatives*, Academic Press, London, 1978.
55. Mehrotra, R.C.; Bohra, R. *Metal Carboxylates*, Academic Press, London, 1983.
56. Doeuff, S.; Henry, M.; Sanchez, C.; Livage, J. *J. Non-Cryst. Solids*, **1987**, *89*, 206.
57. Atik, M.; Aegerter, M.A. *J. Non-Cryst. Solids*, **1992**, *147&148*, 813.

58. Chaumont, D.; Craievich, A.; Zarzycki, J. *J. Non-Cryst. Solids*, **1992**, *147&148*, 127.
59. Debsikar, J.C. *J. Non-Cryst. Solids*, **1986**, *87*, 343.
60. Kundu, D.; Ganguli, D. *J. Mat. Sci. Lett.*, **1986**, *5*, 293.
61. Doeuff, S.; Henry, M.; Sanchez, C.; Livage, J. *J. Non-Cryst. Solids*, **1987**, *89*, 84.
62. Leaustic, A.; Riman, R.E. *J. Non-Cryst. Solids*, **1991**, *135*, 259.
63. Gagliardi, C.D.; Dunuwila, D.; Berglund, K.A. in *Mat. Res. Soc. Symp. Proc.* 180; Zelinski, B.J.J.; Brinker, C.J.; Clark, D.E.; Ulrich, D.R., Eds.; Materials Research Society, Pittsburgh, 1990, 801.
64. Gagliardi, C.D.; Dunuwila, D.; Van Vlierberge-Torgerson, B.A.; Berglund, K.A. in *Mat. Res. Soc. Symp. Proc.* 271, Hampden-Smith, M.J.; Klemperer, W.G.; Brinker, C.J., Eds.; Materials Research Society, Pittsburgh, 1992, 257.
65. Van Vlierberge-Torgerson, B.A.; Dulebohn, J.I.; Berglund, K.A. in *Chemical Processes of Advanced Materials*, Hench, L.L.; West, J.K., Eds.; John Wiley & Sons, Inc., 1992, 415.
66. Severin, K.G.; Ledford, J.S.; Torgerson, B.A.; Berglund, K.A. *Chem. Mat.*, **1994**, *6*, 890.
67. Yoldas, B. E. *J. Mat. Sci.* **1986**, *21*, 1087.
68. Mehrotra, R.C. in *Recent Advances in Inorganic and Radiochemistry*, Sharpe, A.G.; Emeleus, H.J., Eds., Vol. XXVI (Academic Press, New York), 269.
69. Melpoder, S. M.; Cotrain, B. K. *Mater. Res. Soc. Symp. Proc.* **1988**, *121*, 811.
70. Babonneau, F.; Leaustic, A.; Livage, J. *Mater. Res. Soc. Symp. Proc.* **1988**, *121*, 317.
71. Schmidt, H.; Rinn, G.; NaB, R.; Sporn, D. *Mater. Res. Soc. Symp. Proc.* **1988**, *121*, 743.
72. Sanchez, C.; Babonneau, F.; Doeuff, S.; Leaustic, A. in *Ultrastructure Processing of Ceramics, Glasses, and Composites*; Mackenzie, J. D., Ulrich, D. R., Eds.; John Wiley & Sons; New York (1988), p.77.
73. Schmidt, H.; Seiferling, B. in *Mat. Res. Soc. Symp. Proc.*, **1986**, *73*, 739.
74. Sanchez, C.; Livage, J. *New J. Chem.* **1990**, *14*, 513.
75. Gagliardi, C. D.; Berglund, K. A. *Mat. Res. Soc. Symp. Proc.* **1989**, *155*, 127.
76. Teller, H. L. *Sens. and Act.*, **1983**, *4*, 679.
77. Ichinose, N. *Am. Ceram. Soc. Bull.*, **1985**, *64*, 1581.
78. Prassas, M.; Hench, L. L. in *Ultrastructure Processing of Ceramics, Glasses and Composites*, L. L. Hench and D. R. Ulrich Eds., Wiley, New York, 1984, 100.
79. Livage, J. *Mat. Res. Soc. Symp. Proc.*, **1986**, *73*, 717.
80. Doeuff, S.; Henry, M.; Sanchez, C. in *Better Ceramics Through Chemistry II*, C.J. Brinker, D.E. Clark and D. R. Ulrich Eds., Mater. Res. Soc. Symp. Proc., *73*, M.R.S., Pittsburgh, 1986, 653.
81. Komareni, C.; Roy, R.; Breval, E. *J. Am. Ceram. Soc.*, **1985**, *68*, C41.
82. Severin, K. G.; Ledford, J. S. *manuscript in preparation*.
83. Hoffman, L.W., Ledford, J.S. *manuscript in preparation*.
84. Göpel, W.; Kirner, U.; Wiemhöfer, H. D.; Rocker, G. *Solid State Ionics*, **1988**, *28-30*, 1423.

85. Hamasaki, Y.; Ohkubo, S.; Murakami, K.; Sei, H.; Nogami, G. *J. Electrochem. Soc.*, **1994**, *141*(3), 660.
86. Raju, A. R.; Rao, C. N. R. *Sensors and Actuators*, **1993**, *B21*, 23.
87. Boccuzzi, F.; Guglielminotti, E. *Sensors and Actuators*, **1993**, *B21*, 27.
88. Kung H. H., *Transition Metal Oxides: Surface Chemistry and Catalysis*, Elsevier: Amsterdam, 1989.
89. Livage, J.; Holivet, J. P.; Tronc, E. *J. Non-Cryst. Solids*, **1990**, *121*, 35.
90. Livage, J.; Barboux, P.; Badot, J. C.; Baffier, N. in *Better Ceramics Through Chemistry III*; Brinker, J. C.; Clark, D. E.; Ulrich, D. R. Eds.; Mat. Res. Soc. Symp. Proc., **1988**, *121*, 167.
91. Livage, J.; *Chem. Mater.*, **1991**, *3*, 578.
92. Pomonis, P. J.; Vickerman, J. C. *Faraday Discuss.* **1981**, *72*, 247.
93. Carrizosa, I.; Muneura, G. *J. Catal.* **1977**, *49*, 189.
94. Prandtl, W.; Hess, L. *Anorg. Allg. Chem.*, **1958**, 296, 36.
95. Sanchez, C.; Nabavi, M.; Taulelle, F. in *Better Ceramics Through Chemistry III*; Brinker, J.C.; Clark, D.E.; Ulrich, D.R. Eds.; Mat. Res. Soc. Symp. Proc., **1988**, *121*, 93.
96. Nabavi, M.; Sanchez, C.; Livage, J.; *Eur. J. Solid State Inorg. Chem.*, **1991**, *28*, 1173.
97. Livage, J. *Mater. Res. Bull.* **1991** *26*(11), 1173.
98. Inubishi, A.; Masuda, S.; Okubo, M.; Matsumoto, A.; Sadamura, H.; Suzuki, K. in *High Tech Ceramics*; Vincenzini, P. Ed., Elsevier: Amsterdam, 1987; 217.
99. Glezer, V.; Lev, O. *J. Am. Chem. Soc.* **1993**, *115*, 2533.
100. Rushau, G. R.; Newnham, R. E.; Runt, J.; Smith, B. E.; *Sensors and Actuators* **1989**, *20*, 269.
101. Rao, C. N. R. *Talanta* **1992**, *115*, 2533.
102. Rao, N.; van den Bleek, C. M.; Schoonman, J. *Solid State Ionics* **1993**, *59*, 263.
103. Briggs, D.; Seah, M. P. *Practical Surface Analysis*, 2nd ed. Wiley: New York, **1990**.
104. Woodruff, D. P.; Delchar, T.A.; *Modern Techniques of Surface Science*, Cambridge University Press: New York, **1989**.
105. Werthiem, G. K. in *Solid State Chemistry Techniques*, Cheetham, A. K.; Day, P.; eds.; Claredon Press; Oxford, **1987**.
106. Scofield, J. H. *J. Electron Spectrosc. Relat. Phenom.* **1976**, *8*, 129.
107. Penn, D. R. *J. Electron. Spectrosc. Relat. Phenom.* **1976** *9*, 29.
108. Skoog, D. A.; West, D. M.; Holler, F. J. *Analytical Chemistry: An Introduction*, 4th ed., Saunders College Publishing, Orlando, FL, 1990.
109. Drago, R. S. *Physical Methods for Chemists*, 2nd ed., Saunders College Publishing, Orlando, FL, 1992.
110. Niemantsverdriet, J. W. *Spectroscopy in Catalysis*, VCH Publishers, New York, 1993.
111. Ibanez, J. G.; Solorza, O.; Gomez del-Campo, E. *J. Chem. Ed.* **1991** *68*(10), 872.
112. Bragg, W. L. *Proc. Camb. Phil. Soc.*, **1912**, *17*, 43,
113. Scherrer, P. *Gött. Nachr.* **1918** *2*, 98.

- 114. Klug, H. P.; Alexander, L. E. *X-Ray Diffraction Procedures for Polycrystalline and Amorphous Materials*, 1st Ed. Wiley: New York, 1954.
- 115. Cohen, J. B. *Ultramicroscopy* **1990** 34, 41.

Chapter 2

Effects of Annealing Temperature on the Structure of Vanadium Oxide/Titanium Oxide Thin Films Derived from Metal Carboxylate Sol-Gel Processing

2.1 Introduction

The semiconducting properties of titanium dioxide have been widely studied. A large portion of current research involving TiO_2 is being directed towards the development of chemical sensors based on its semiconducting properties [1-3]. An important step in the development of chemical sensors is to study the active phase of the V/Ti oxide system with respect to its semiconducting properties. Before sensing properties can be studied, suitable materials must be developed.

This chapter presents the first of a two-part study conducted to investigate the influence of vanadium on the structure of titanium oxide thin films. Titanium dioxide films doped with 10 mole % vanadium were prepared via the sol-gel technique. Preparation involved the hydrolysis of metal alkoxides using excess valeric acid at room temperature. The structures of these films were changed by varying the temperature at which the films were annealed. Surface and bulk film structures were studied using XPS, XRD, FTIR and UV-Vis spectroscopies. Results obtained by XRD agree with data presented in earlier studies indicating that the presence of vanadium promotes the crystallization of titanium oxide [4]. No crystallization of vanadium was found at elevated temperatures, as evident

through XRD patterns and FTIR spectra. Results obtained by XPS indicate that temperature has an influence on the amount as well as the phase of vanadium present in the surface of these films. UV-Vis findings support XPS findings, as well as provide information on the coordination of vanadium atoms in the films. UV-Vis data will also show that annealing temperature significantly affects the band gap of TiO_2 in the films.

The properties of V/Ti catalysts prepared by impregnating the TiO_2 support with vanadia species have been studied [5]. Many of the recent studies using V/Ti catalysts have involved the oxidation of hydrocarbons [6,7] and the reduction of nitric oxide by ammonia [8-10]. The activity of these catalysts has been attributed to the surface phase of the vanadia species. High surface area and controlled porosity (which are hard to control with traditional catalyst preparation methods) influence the quality of the sensor. Sol-gel technology offers more control over these properties of the resulting material, giving materials prepared via sol-gel chemistry advantages over materials produced through traditional methods. In addition to controlled surface area and porosity, the electronic properties can be enhanced through the mixing of metal oxides [11] or by annealing the oxide materials at various temperatures [12]. Thus, sol-gel methods using titanium and vanadium alkoxides to produce mixed metal oxides may prove to be advantageous for the preparation of chemical sensing materials [13-15].

The oxide network obtained through sol-gel preparations is attractive since homogeneous multi-component systems can be achieved through the mixing of precursors [17]. Temperatures for processing can be low, making chemical modifications easier and low processing temperatures can lead to a wide range of new properties [16]. Therefore,

much attention has been directed towards understanding the hydrolysis and condensation of silicon and transition metal alkoxides [17,18]. Modifying the alkoxides with carboxylic acids before hydrolysis increases the quality of the films produced from alkoxide precursors. Slower condensation rates are obtained by carboxylic acid complexation of the metal alkoxide precursors. The slower rates are important for producing polymeric gels as opposed to solid oxide precipitates [16]. Valeric acid modified alkoxides produce sols from which films can be cast that are uniform, transparent, and that adhere well to quartz substrates [19,20].

It has been proven that both the temperature at which these systems are treated as well as the amount of vanadium present affect the final structure of the product. Machej *et al.* [21] have reported that the metal oxide-oxide surface interaction of V/Ti catalysts is affected by different annealing temperatures. The structure and composition of V/Ti catalysts have been studied previously as a function of temperature [4]. These authors found that the structural transformation of the TiO_2 support from anatase to rutile and the morphology of the supported vanadium phase were functions of temperature. The impregnation of the support with the vanadium salt results in the formation of vanadyl oxalate at low temperatures. Raising the calcination temperature initially leads to the presence of V_2O_5 crystals before the supported vanadia phase reacts with the TiO_2 (anatase) to produce a $\text{V}_x\text{Ti}_{1-x}\text{O}_2$ (rutile) solid solution.

To date, work involving vanadium oxide/titanium oxide thin films prepared through the sol-gel process has not appeared in literature. The goal of the research presented in this chapter was to study the effect of annealing temperature on the surface and bulk

phases of vanadium oxide/titanium oxide thin films produced via sol-gel technology. In the following chapter, the effect vanadium loading has on film structure is presented. Results from these two studies will be used to determine the feasibility of sol-gel produced vanadium oxide/titanium oxide thin films for use as conductimetric sensors.

2.2 Experimental

Materials. Titanium (IV) isopropoxide (97%, Aldrich Chemical Co.), valeric acid (99+%, Aldrich Chemical Co.), and vanadium triisopropoxide oxide (Gelest Inc.) were used without further purification. Distilled, deionized water was used for all preparations.

Solution Preparation. The method used to prepare the films was adapted from one previously developed for titanium compounds [20]. Since both metal precursors are easily hydrolyzed, solutions were prepared in a glovebox under continuous N₂ purge. In the glovebox, the reactions were carried out at room temperature in capped vials. The sols were prepared such that there was 10 mole % vanadium in titanium. The metal:water:acid ratio was 1:1.5:9. Vanadium triisopropoxide was added to titanium (IV) isopropoxide followed by the addition of valeric acid and then water. The solution was vigorously shaken with a vortex mixer following the addition of each reactant. Solutions were prepared in duplicate.

When the two metal precursors were initially mixed, no apparent change was observed and the solution remained colorless. When the acid was added, an immediate

color change to bright yellow was observed. Finally, when water was added, there was a further color change to a dark yellow-orange.

Film Preparation. Solutions were deposited on a quartz substrate, spun for a minimum of 5 minutes and air-dried overnight. Next, the films were dried for 6 hours at 100°C in a tube furnace under the flow of dry air (100 cc/min, medical grade, AGA Gas). Each film was then annealed at the desired temperature for 24 hours under the same conditions (dry air, 100 cc/min). Film preparations from each solution were carried out in triplicate. An as-cast film, meaning unheated, from each solution was analyzed in order to confirm solution/film reproducibility.

Reference films were prepared containing vanadium oxide and titanium oxide separately. These films were prepared in a manner similar to those containing both vanadium and titanium. The film containing vanadium oxide was annealed at 500°C for 4 hours. The titanium oxide films were annealed at 600°C to obtain films containing crystals primarily in the anatase phase and at 1000°C to obtain a mixture of anatase and rutile crystals, although the films still remained highly amorphous. The titanium films were also annealed for 4 hours.

Fourier Transform Infrared Spectroscopy (FTIR). FTIR spectra were collected from films that were spin coated on KBr windows, using a Mattson Instruments Galaxy 3020 Fourier transform infrared spectrometer. Data were obtained in mid-IR region (4000 - 400 cm^{-1}) with a resolution of 2 cm^{-1} . Data acquisition was performed using an Enhanced First software package.

X-ray Photoelectron Spectroscopy (XPS) Films cast on quartz slides were analyzed with a VG Microtech spectrometer using a Clam2 hemispherical analyzer. Data were collected with a Mg anode operated at 15 kV and 20 mA (300W) and an analyzer pass energy of 50 eV. The core regions for four elements were scanned with each film: C 1s, O 1s, Ti 2p_{3/2} and V 2p_{3/2}. Binding energy charge corrections for films containing Ti were made with reference to the Ti 2p_{3/2} peak (458.5 eV [22]). Corrections for reference films of V₂O₅ were made with reference to C 1s (284.6 eV). The binding energies given have a precision of ± 0.1 eV. Quantitative measurements were performed using sensitivity factors determined previously [23]. For quantitative determination of the V 2p_{3/2} region, the contribution from the O 1s satellite was subtracted out from the area attributed to V 2p_{3/2} before calculations were made. Curve fitting was performed using a 20% Lorentzian-Gaussian mix Voigt function [24].

X-ray Diffraction (XRD). All films were analyzed with a Rigaku XRD diffractometer using Cu K α radiation ($\lambda = 1.5418$ Å). The X-ray tube was operated at 45 kV and 100 mA. The diffractometer was scanned at a rate of 0.07 deg/min (deg = 2θ). Divergence and scattering slits were both set at 1°. Since quartz shows a broad absorbance contributing to data at the lower end of the scanned region, information for a blank quartz slide was obtained and subtracted from the XRD data collected for each film.

Ultraviolet-visible spectroscopy (UV-Vis). A Unicam UV-Vis spectrometer was used to collect UV-Vis spectra. The incident beam was normal to the surface of the film using a blank quartz slide as a reference. Data were collected using Vision software in absorbance mode with a bandwidth of 2 nm and a data interval of 1 nm.

2.3 Results and Discussion

FTIR. Normalized spectra representative of the V/Ti and Ti films calcined at 400°C are shown in Figure 2.1. No features attributable to valerate ligands are present indicating they have been removed during calcination. The titanium oxide thin film spectrum (Figure 1b) contains a major peak at 448 cm^{-1} that is attributed to a titanium-oxygen stretch. The spectrum recorded for the V/Ti film (Figure 1b) also contains the band at 447 cm^{-1} due to the titanium-oxygen stretch. The feature at 944 cm^{-1} is indicative of an absorbance from a partially hydrated surface $\text{V}=\text{O}$. The broad absorption centered at 796 cm^{-1} is attributed to VO-V stretching modes of the V-O-V bonds [25]. The shoulders at 890 cm^{-1} for the $\text{V}=\text{O}$ stretch and 715 cm^{-1} for the VO-V stretch suggest the presence of a reduced vanadium species. Using data reported Nyquist and Kagel [26], the features occurring at 796 and 890 cm^{-1} can be attributed to oxides of V^{5+} while the shoulders on both peaks appearing at a slightly higher frequency can be attributed to oxides of V^{4+} . Thus, IR data indicates the presence of more than one oxidation state for vanadium with V^{5+} being more abundant.

V_2O_5 crystals have two characteristic absorbances at 1020 and 940 cm^{-1} , attributed to the $\nu\text{V}=\text{O}$ of crystalline V_2O_5 and the symmetric stretch of V_xO_y clusters, respectively [27]. Since no feature at 1020 cm^{-1} is observed, our FTIR data suggests that no crystalline V_2O_5 is present in the film. Busca *et al.* [27] report that surface vanadium will be amorphous at low loadings, and amorphous and crystalline for higher loadings. Wachs [28] showed that crystalline V_2O_5 IR absorption always occurs at 1020 cm^{-1} and surface

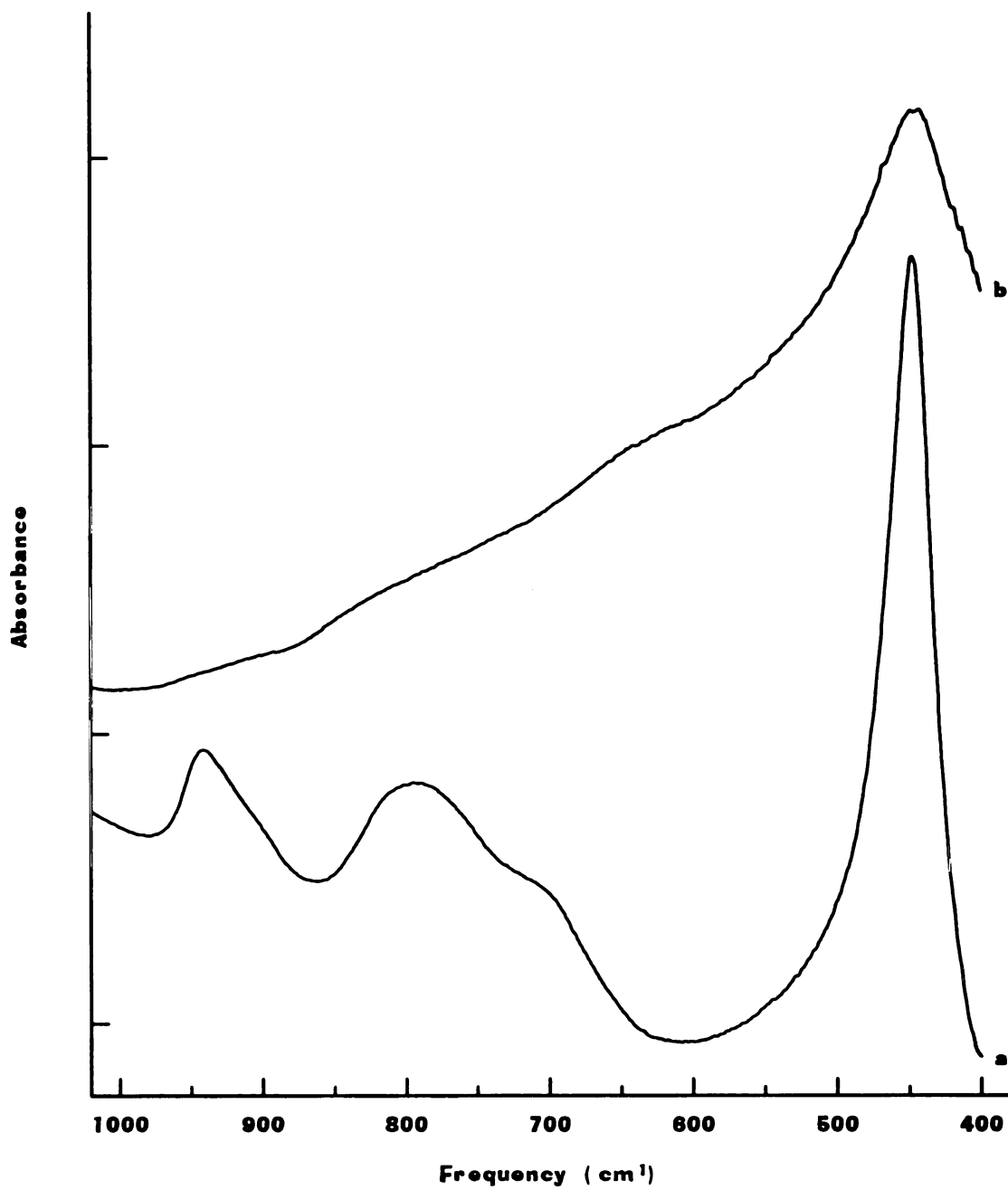


Figure 2.1. FTIR spectra of (a) V/Ti film annealed at 400°C and (b) Ti film annealed at 400°C.

vanadium oxide species will adsorb between $800\text{-}995\text{ cm}^{-1}$ for a hydrated surface. Thus, our results suggest only a partially hydrated surface vanadium species is formed without crystalline vanadium oxide.

XRD. XRD patterns of the V/Ti films are shown in figure 2.2. The range selected ($2\theta = 24.00 - 29.00$) shows the most intense peaks for both TiO_2 anatase ($2\theta = 25.30$) and rutile ($2\theta = 27.45$). Intense peaks for penta- and tetra-valent vanadium oxides also occur in this region: $2\theta = 26.21$ for V_2O_5 and 27.88 for V_2O_4 . Background due to the quartz substrate has been subtracted from each of the patterns. The as-cast film (not shown) and the film annealed at 300°C (2.2a) were featureless. At 400°C (2.2b) a broad feature centered at $2\theta = 25.3$ is present. After annealing the film at 500°C (Figure 2.2c), the feature at $2\theta = 25.3$ narrows and a new feature at $2\theta = 27.5$ can be observed. Finally at 600°C (2.2d), the feature at $2\theta = 25.3$ continues to narrow and the feature at $2\theta = 27.5$ increases significantly.

At the lowest temperatures, figure 2.2a, the absence of any feature in the XRD patterns suggests that the film is amorphous. The feature in the 400°C calcined film at $2\theta = 25.3$ (2.2b) suggests the formation of TiO_2 (anatase) crystals while features due to both anatase ($2\theta = 25.3$) and rutile ($2\theta = 27.5$) appear when the film is annealed at 500°C (2.2c). The relative concentration of TiO_2 (rutile)/ TiO_2 (anatase) increases as the annealing temperature is further increased to 600°C (2.2d). Information provided by XRD has shown the formation and phase transformation of TiO_2 crystals in our films. Our data do not show formation of V_2O_5 crystals.

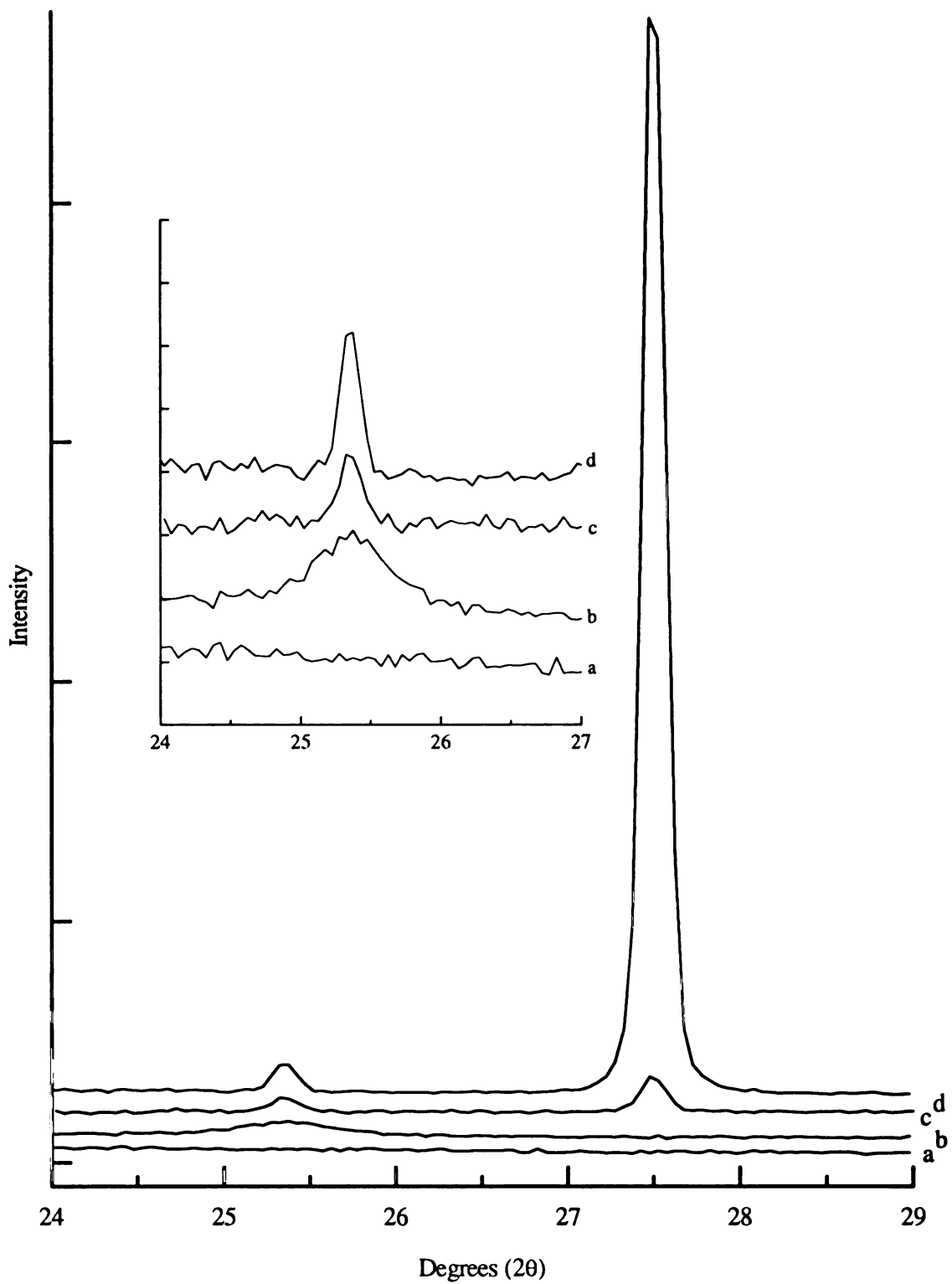


Figure 2.2. XRD patterns measured for V/Ti films annealed at (a) 300°C, (b) 400°C, (c) 500°C, and (d) 600°C.

As observed by the inset in figure 2.2, narrowing of the $\text{TiO}_2(\text{anatase})$ XRD feature occurs with increased annealing temperature. The narrowing of the anatase feature suggests that the particle size of this phase grows with temperature. The particle sizes for each of the films, as determined through the Scherrer equation [29], are presented in table 2.1. The mean particle size of $\text{TiO}_2(\text{anatase})$ significantly increases from 143.4 Å after initially being detected at 400°C to 545.0 Å when the film is annealed at 600°C. Although the relative intensity of the $\text{TiO}_2(\text{rutile})$ feature significantly increases with temperature (figs. 2.2c and 2.2d), the mean particle size remains constant at approximately 542 Å.

Table 2.1. Particle size of TiO_2 crystals in V/Ti thin films. Calculations were made using FWHM of respective XRD feature.

temp	anatase			rutile		
	peak pos.	FWHM	size (Å)	peak pos.	FWHM	size (Å)
as cast	---	---	---	---	---	---
300 C	---	---	---	---	---	---
400 C	25.4	0.578	143.4	---	---	---
500 C	25.3	0.184	451.3	27.5	0.154	542.8
600 C	25.4	0.153	545.0	27.6	0.153	542.4

The data collected by XRD shows the formation of TiO_2 crystals, which agrees with the information obtained from infrared spectroscopy. XRD also provides information about the resulting phase of TiO_2 . The predominance of the peak at $2\theta = 27$ for films calcined at 600°C (spectrum d) suggests a significant formation of $\text{TiO}_2(\text{rutile})$ as compared to that of $\text{TiO}_2(\text{anatase})$. Saleh *et al.* [4] studied 7% V/Ti catalysts calcined

over the temperature range 110-750°C. In their work, the vanadia species were introduced through wet impregnation to TiO₂(anatase). A significant amount of the anatase phase was transformed to rutile at 700°C. For samples heated between 350 and 650°C, Saleh *et al.*, reported the appearance of a very weak peak which they attributed to crystalline V₂O₅. Busca *et al.* [27] did not observe crystalline V₂O₅ in their XRD patterns collected for a 9% w/w sample calcined at 720°C. However, Busca reported the presence of a V₂O₅ peak in an XRD pattern when increasing the V₂O₅ loading to 15% w/w. Earlier studies performed on sol-gel derived TiO₂ thin films [30] indicate the phase transformations from amorphous to anatase and anatase to rutile occur at temperatures of 600° and 1000°C, respectively. In comparison, our data show the presence of vanadia species influences the crystallization and phase transformation of titanium.

Wachs *et al.* [31] reported that crystalline V₂O₅ is formed only after the complete formation of a monolayer over the TiO₂(anatase) support. Saleh *et al.* [4] took this further by stating that crystalline V₂O₅ initiates the formation of V_xTi_{1-x}O₂ (rutile) from the supported vanadia phase on TiO₂(anatase). In our studies of thin films derived from sol-gel chemistry, we have shown that the initial transformation of amorphous Ti to anatase, and then further transformation of anatase to rutile at a lowered temperature did not require the presence of crystalline V₂O₅.

UV-Vis. For reference, figure 2.3 contains UV-Vis data collected from highly amorphous TiO₂ thin films containing anatase (2.3a) or anatase and rutile (2.3b) crystal structures. Determination of the crystal phase present in each film was obtained from XRD data collected on these films. The broad absorbance below 350 nm in both 2.3a and

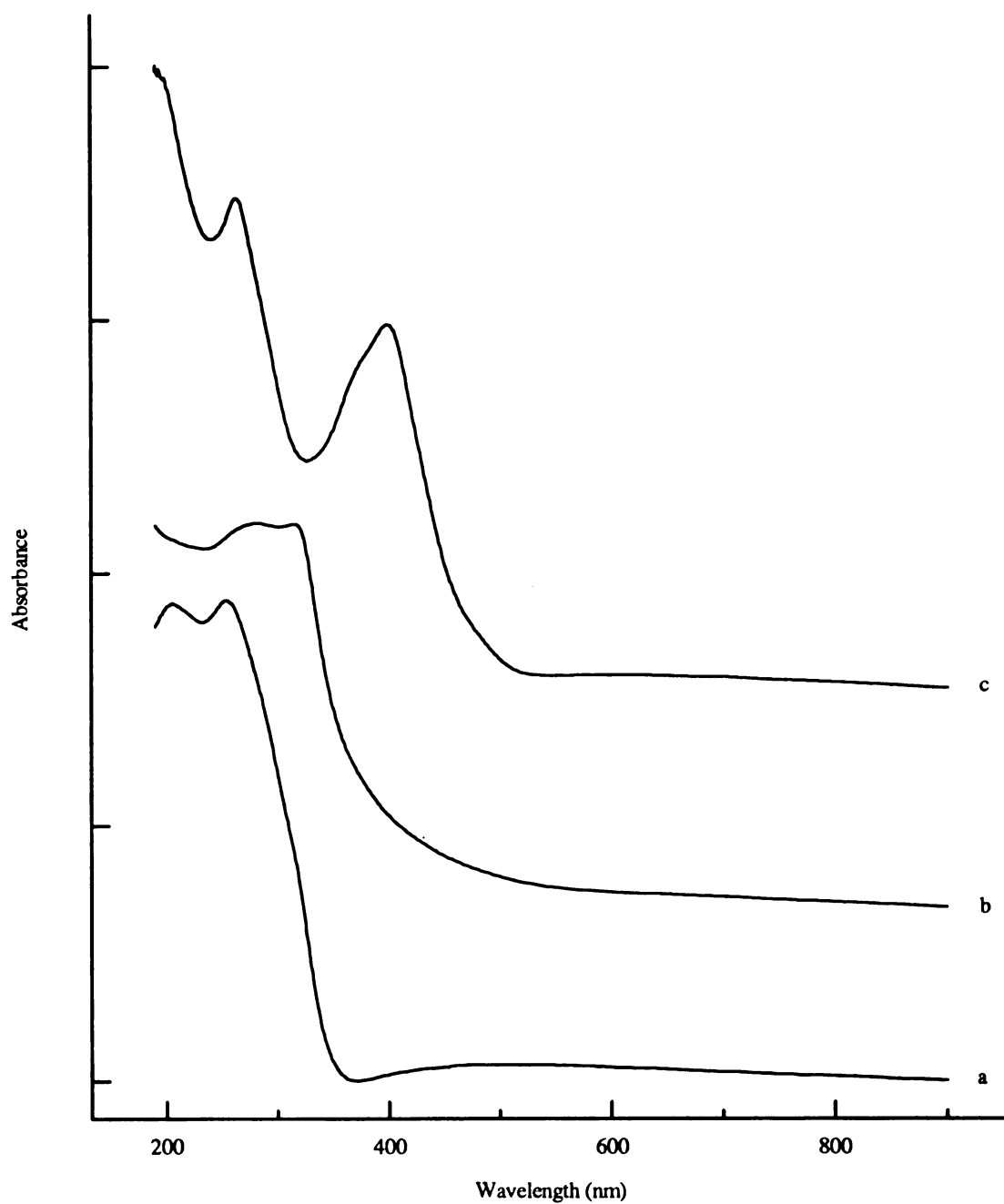


Figure 2.3. UV-Vis spectra collected for primarily amorphous thin films containing the following crystalline phases (a) TiO_2 (anatase), (b) TiO_2 (anatase) and TiO_2 (rutile), and (c) V_2O_5 .

2.3b can be attributed to an electronic transition from the valence to conduction band of TiO_2 [32]. Conduction band edges were determined for TiO_2 anatase and rutile to be 3.57 eV and 3.36 eV, respectively. A band gap of 3.44-3.51 eV has been reported for a fully crystallized rutile thin film [33]. The band gap for the material in the present study is slightly less than that of rutile indicating a poorly crystallized or highly amorphous thin film [34,35]. Figure 2.3 also contains the spectrum from a film primarily composed of V_2O_5 (2.3c). The absorbances observed for the vanadium oxide film are a result of charge transfer from vanadium to terminal oxygen [33]. Schraml-Marth *et al.* [36] report tetrahedrally coordinated vanadium(V) has a charge transfer transition in the 285-335 nm region while the charge transfer transition for octahedrally coordinated vanadium(V) occurs in the 400-500 nm region. The differences in energies in our spectrum of vanadium oxide suggest differences in the coordination of vanadium, where absorbances at 400 and 265 nm represent vanadium in its +5 oxidation state with octahedral and tetrahedral coordinations, respectively.

Figure 2.4 shows the UV-Vis data collected for films calcined at the indicated temperatures. The spectra for both samples calcined at 300°C and 400°C are similar. A strong absorbance due to TiO_2 is observed below 350 nm and the shoulder at 390 nm is attributed to octahedrally coordinated vanadium(V). A broad, weak absorption in this spectrum occurs between 478 and 900 nm. Schraml-Marth *et al.* [36] have suggested that octahedrally coordinated vanadium(IV) absorbs with a broad transition between 625 and 770 nm. Flynn and Pope [37] attributed a peak near 1100 nm to an “intervalence charge transfer transition” for a mixed valence compound. Thus, we can attribute this broad peak

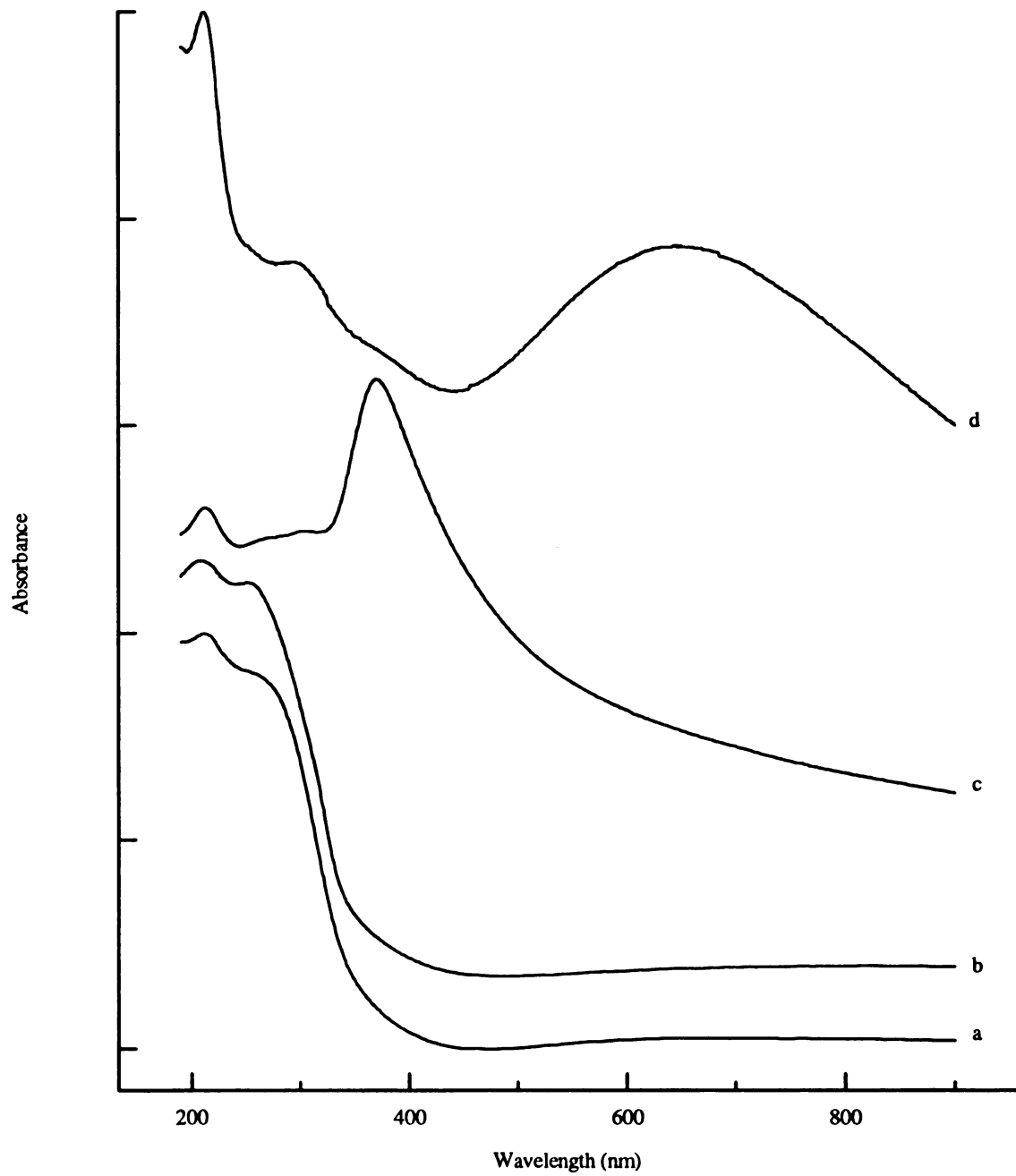


Figure 2.4. UV-Vis spectra obtained for V/Ti films annealed at (a) 300°C, (b) 400°C, (c) 500°C, and (d) 600°C.

at the lower energy to vanadium(IV) in an octahedral environment as well as charge transfer between V(IV) and V(V). The band edge of TiO₂ for both the films calcined at 300°C and 400°C is observed at 3.54 eV, which is similar to that of TiO₂(anatase). The film calcined at 500°C shows an increased absorption due to octahedrally coordinated V(IV). In addition, the band edge for TiO₂ is shifted to 3.41 eV, which indicates a shift towards the band edge indicative of TiO₂(rutile). The film calcined at 600°C (Figure 2.4d) shows a dramatic increase in the absorption due to V(IV) in an octahedral environment. This is accompanied by a decrease in the size of the feature between 360 and 440 nm. Although the absorption between 360 and 250 nm due to TiO₂ is still present, a collapse of the band edge is observed for the 600°C films that can be attributed to a formation of the solid solution V_xTi_{1-x}O₂.

XPS. XPS findings have been summarized in table 2.2. A small feature due to adventitious carbon was observed in all spectra at 284.6 eV. The O 1s spectra measured for the films consists of an intense feature due to backbone oxygen (530.0 eV) while a

Table 2.2. Binding energies of V 2p_{3/2} features as a function of calcination temperature. V₂O₅ refers to data collected from a vanadium oxide standard.

Sample	Binding Energy	V 2p _{3/2}	FWHM V 2p _{3/2}
V/Ti ascast	515.1		2.435
300°C	516.4		3.122
400°C	516.6		2.718
500°C	517.0		2.668
600°C	517.0		2.846
V ₂ O ₅	517.1		

shoulder appears at ~2 eV higher binding energy indicating a small amount of water adsorbed on the surface.

The affect of temperature on the V $2p_{3/2}$ binding energy is presented in figure 2.5. Along with the spectra obtained from films calcined at various temperatures, a spectrum showing the V $2p_{3/2}$ feature from an as-cast film (Figure 2.5a) as well as the spectrum collected from a V_2O_5 standard (Figure 2.5f) have been included. The V $2p_{3/2}$ binding energy of 517.1 eV observed in our V_2O_5 standard corresponds to the generally accepted value for vanadium in its +5 oxidation state [38]. The XPS spectrum collected from the valerate films shows a V $2p_{3/2}$ centered at 515.2 eV indicating the presence of a reduced vanadium species [38]. XPS data show the V $2p_{3/2}$ feature shifting to higher binding energies as the annealing temperature is increased to 500°C, suggesting that the surface vanadium species is being oxidized. At 600°C, however, a shift to lower binding energy of the vanadium feature suggests some of the fully oxidized vanadium is now being reduced.

The FWHM of the V $2p_{3/2}$ feature was also studied as a function of temperature. The results indicate an initial increase of the linewidth from 2.44 eV in as-cast samples to 3.12 in samples calcined at 300°C. Further annealing resulted in a decreased FWHM for films calcined at 400 and 500°C while films calcined at 600°C showed a slight increase in FWHM over that from 500°C calcined films.

The V $2p_{3/2}$ feature from as-cast films is primarily due to the presence of both V^{4+} and V^{3+} [38]. The relative ratio of V^{4+} to V^{3+} , calculated from the relative areas of the fitted peaks, is approximately 2:1. The shift of the V $2p_{3/2}$ peak to higher binding energies

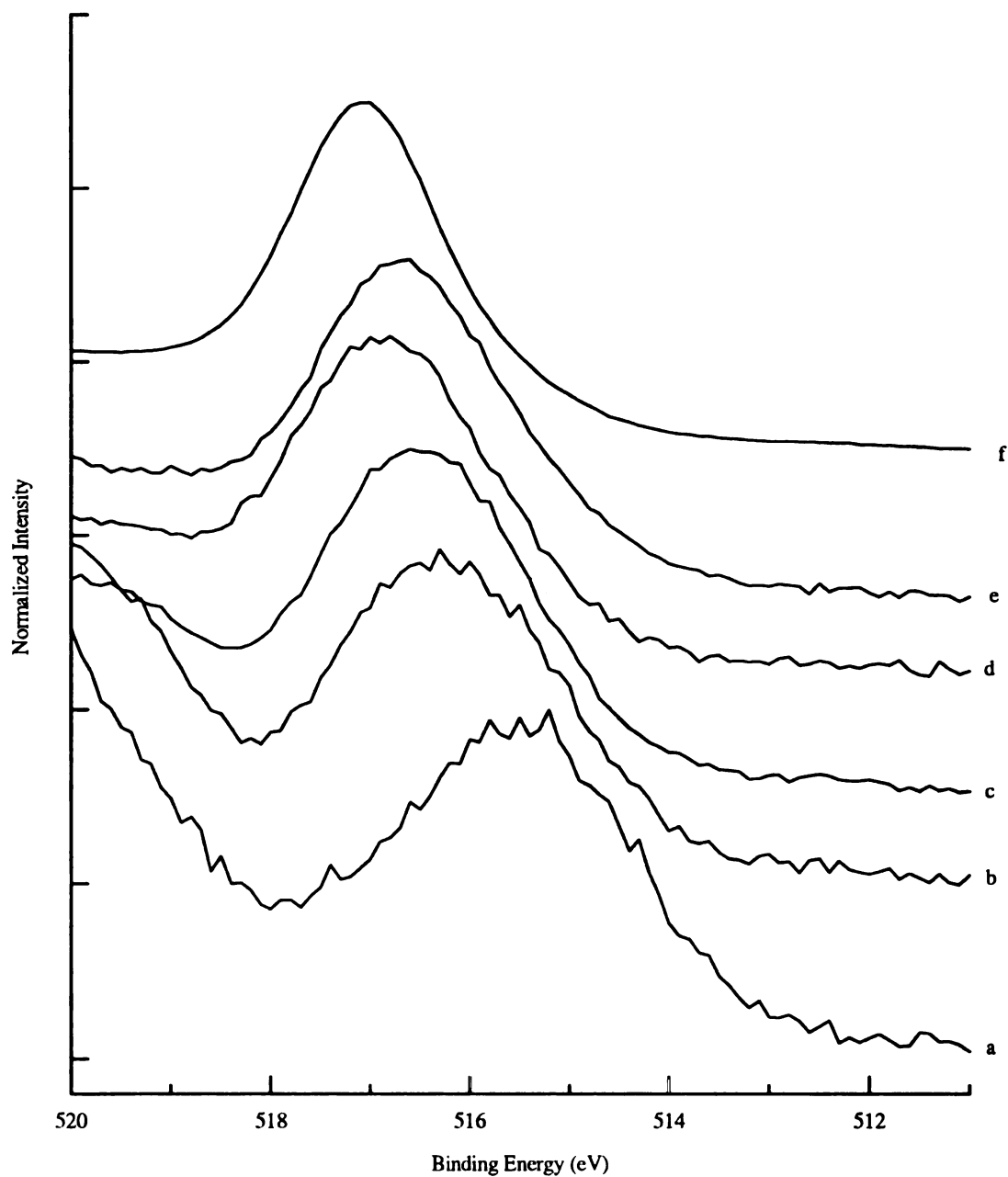


Figure 2.5. Vanadium 2p_{3/2} photoelectron spectra collected for V/Ti films (a) ascast, films annealed at (b) 300°C, (c) 400°C, (d) 500°C, and (e) 600°C and a reference spectra of V₂O₅ (f).

and the subsequent (initial) increase in FWHM upon initial calcination of the thin films suggests the vanadium species are primarily in their 4+ and 5+ oxidation states. Further shift of the V 2p_{3/2} to an even higher binding energy with a continuous decrease in linewidth (with the exception of the 600°C calcined film) suggests that the V in the films continue to oxidize to the most stable state of V⁵⁺. At 600°C, the increase in the FWHM of V 2p_{3/2} feature indicates an increased presence of V⁴⁺ in the surface of the film. To our knowledge, results indicating the V 2p_{3/2} binding energy shifting as a function of temperature have not appeared previously in literature, although the shifting of V 2p_{3/2} binding energy as a function of loading has been studied [39]. This additional presence of V⁴⁺ at high temperatures could support an explanation of the formation of a solid solution of V_xTi_{1-x}O₂(rutile).

The V/Ti surface ratio obtained from XPS analysis of samples heated between 300 and 600°C is presented in figure 2.6. The ratio of 0.1 from samples heated to 300°C doubled to 0.2 when the sample was heated to 400°C. The V/Ti ratio doubled again when the sample was heated to 500°C (0.4). Finally, a significant increase in the ratio to 1.1 is observed when the films were calcined at 600°C. There are two situations associated with such a growth of the surface V/Ti ratio. First, the crystal structure of TiO₂ will influence the surface ratio of V/Ti in the film. Growth of TiO₂ particles will lead to phase separation. Vanadium is known to spread well on the TiO₂ surface, coating the outside of the crystals. The XRD data presented earlier showed the films were completely amorphous at 300°C, leaving the V species well dispersed *in* the amorphous TiO₂ (XRD also showed no formation of crystalline TiO₂). At 400°C, XRD showed the formation of

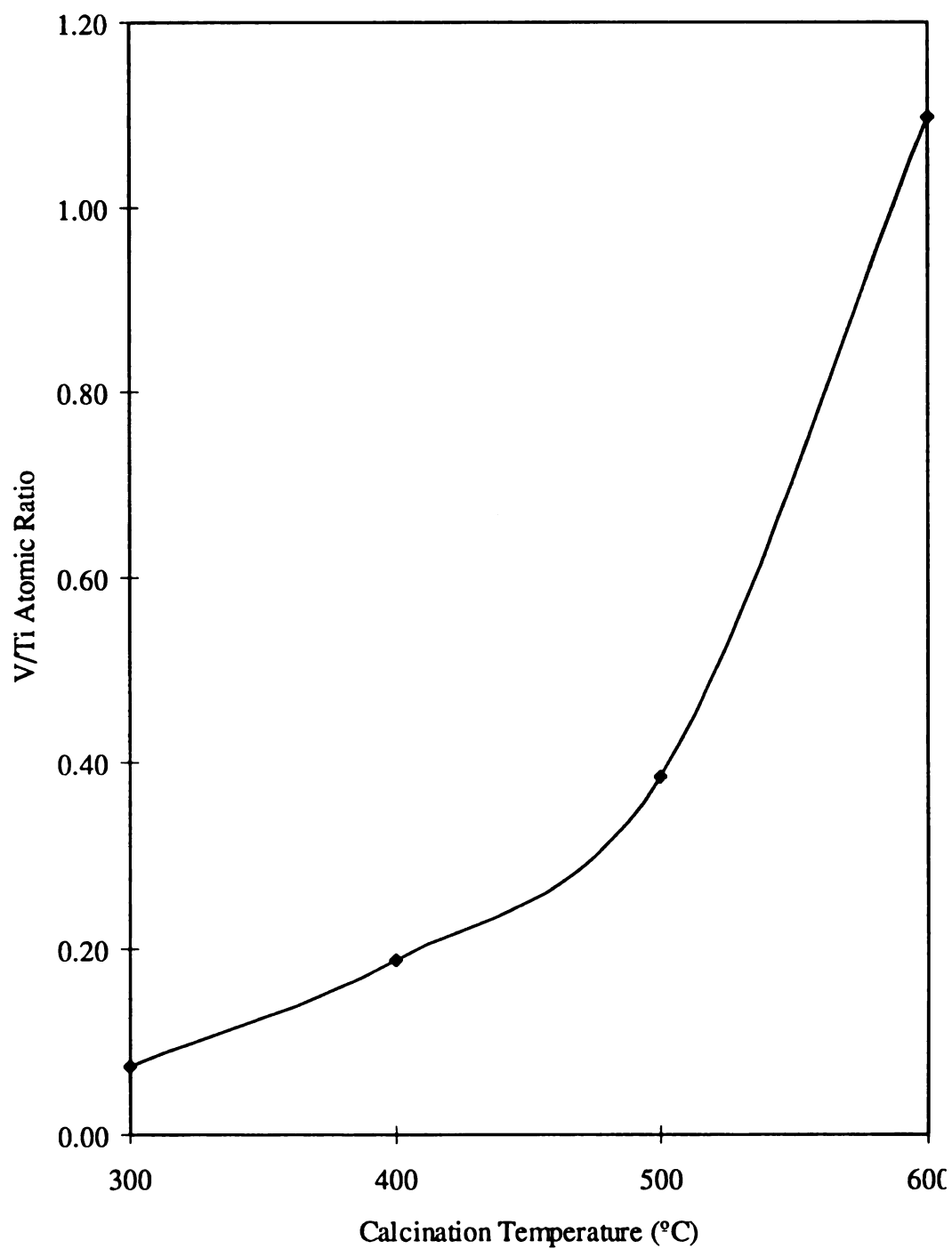


Figure 2.6. Variation in XPS determined V/Ti atomic ratio as a function of annealing temperature.

small amount of TiO_2 (anatase), making it likely that the V species was dispersed *on* these crystals. The formation of the larger TiO_2 (rutile) phase at 500°C makes it possible for the V species to spread, further increasing the value of V/Ti as the V ‘coats’ the TiO_2 particles. The dramatic increase in the V/Ti ratio observed from the 600°C calcined film (1.1) compared to that of 500°C film (0.4) correlates well with the information obtained through XRD. The significant increase of TiO_2 (rutile) phase at 600°C allows the amorphous V species to spread well on the surface of the TiO_2 crystals thus significantly reducing the amount of Ti observed by XPS.

The second consideration involves the oxidation state of vanadium. As discussed above, the increase in annealing temperature used to treat the thin films causes oxidation of the vanadium species. The increased oxidation occurs in parallel with the migration of the vanadium species to the surface of the film. Saleh *et al.* [4] showed a trend for the V/Ti ratio increasing over the temperature range 110 - 650°C . A similar trend for temperatures between 300 and 600°C was also apparent in our samples. However, the change for this ratio was more than double in magnitude as compared to results presented by Saleh *et al.*

2.4 Conclusions

Bulk and surface characterization techniques have allowed us to investigate the structure of V/Ti mixed oxide thin films as a function of temperature. Temperature affects both the titanium structure and the vanadium phase within the films. We have shown the

initial transformation of amorphous TiO_2 to TiO_2 (anatase) and further transformation from the anatase to rutile structure occurring at lower temperatures when vanadium was introduced. Introduction of vanadium resulted in a shift of the TiO_2 band gap at low temperatures and a collapse of the band gap at higher temperatures. Through the annealing process, the surface vanadium was oxidized through V(IV) to primarily V(V). The V/Ti ratio on the surface of these films also increased with increased annealing temperature, indicating the migration of the vanadium species to the surface at higher temperatures. XRD and IR indicate the migration with increased temperature does not coincide with the formation of V_2O_5 crystallites. UV-Vis along with XPS data indicate that the bulk of the vanadium coexists in the oxidation states V^{4+} and V^{5+} . Our studies indicate the matrix $\text{V}_x\text{Ti}_{1-x}\text{O}_2$ (rutile) can be obtained without the presence of crystalline V_2O_5 when starting with metal alkoxide precursors.

The results of our work are similar to those already presented. However, with the use of sol-gel technology, films can be obtained at lower temperatures with phase transformations being carried out to a greater extent - giving better control over the entire process. Also, the mechanism by which phase transformation occurs has been altered.

2.5 List of References

1. Satade, K.; Katayama, A.; Ohkoshi, H.; Nakahara, T.; Takeuchi, T. *Sens. Act. B* **1994** *20*, 111.
2. Bocuzzi, F.; Guglielminotti, E. *Sens. Act. B* **1994** *21*, 27.
3. Shimizu, Y.; Kazushi, F.; Takao, Y. Egashira, M. *Sens. Act. B* **1993** *13-14*, 623.
4. Saleh, R. Y.; Wachs, I. E.; Chan, S. S. and Chersich, C. C.; *J. Catal.*, **1986** *98*, 102.
5. Zhang, Z. and Henrich, V. E., *Surf. Sci.*, **277** (1992) 263. Gaior, M.; Gasior, I.; and Grzybowska, G.; *Appl. Catal.* **1984** *10*, 87.
6. Rao, C. N. R.; Raju, A. R.; and Vijayamohanan, K., Gas-sensor Materials in *New Materials*, S.K. Joshi, C.N.R. Rao, R Rsruta and S. Nagakura (eds.), New Delhi, India, 1992, pp. 1-37.
7. Martin, C.; Rives, V.; Sanchez-Escribano, V.; Busca, G.; Lorenselli, V.; and Ramis, G., *Surf. Sci.* **1991** *251/252*, 825.
8. Tufano, V. and Turco, M., *Appl. Catal.* **1993** *B2*, 9.
9. Turco, M.; Lisi, L.; Pirone, R.; *Appl. Catal.* **1994** *B2*, 133.
10. Went, G. T.; Leu, L.-J., Rosin, R. R.; and Bell, Alexis T.; *J. Catal.* **1992** *134*, 492.
11. Yamazoe, N. *Sens. Act. B* **1991** *5*, 7.
12. Morrison, S. R. *Sens. Act.* **1987** *12*, 425.
13. Yoldas, B.E. *J. Non-Cryst. Solids* **38/39** (1980) 81.
14. Wark, T. A.; Gulliver, E. A.; Jones, L.C.; Hampden-Smith, M.J.; Rheingold, A. L.; Huffman, J. C. in *Better Ceramics Through Cemistry IV*, Zelinsky, B. J. J.; Brinker, C. J.; Clark, D. E.; Ulrich, D. R., Eds.; Mater. Res. Soc. Proc. 180; Pittsburg, PA (1990) 61.
15. Wellbrock, U.; Beier, W.; Frischat, G.H. *J. Non-Cryst. Solids* **1992** *147,148*, 350.
16. Sanchez, C.; Livage, J. *new J. Chem.* **1990** *14*, 513
17. Livage, J.; Henry, M.; Sanchez, C. *Prog. Solid State Chem.* **1989** *18*, 259.
18. Brinker, C. J.; Scherer, G. *sol-Gel Science*; Academic Press: San Diego, 1990.
19. Gagliardi, C. D.; Berglund, K. A. in *Better Processing Science of Advanced Ceramics*, Askay, K. A.; McVay G. L.; Ulrich, D. R., Eds.; Mater. Res. Soc. Proc. 180; Pittsburg, PA (1986) 127.
20. Gagliardi, C. D.; Dunuwila D.; Berglund, K. A. in *Better Ceramics Through Chemistry IV*, Zelinsky, B. J. J.; Briker, C.J.; Clark, D. E.; Ulrich, D. R., Eds.; Mater. Res. Soc. Proc. 155; Pittsburg, PA (1990) 801.
21. Machej, T.; Haber, J.; Turek, A. M.; and Wachs, I. E., *Appl. Catal.* **1991** *70*, 115.
22. Wagner, C. D.; Riggs, M. W.; Davis, L. E.; Moulder, J.; Muilenberg, G. E. *Handbook of X-Ray and Photoelectron Spectroscopy*, Physical Electronics Industries, Eden Prairie, MN, 1979.
23. Severin, K. G.; Ledford, J. S. *unpublished results*.
24. Software provided by Dr. Andrew Proctor, University of Pittsburgh, Pittsburgh, PA.
25. Cristiani, C.; Forzatti, P. and and Busca, G.; *J. Catal.* **1989** *116*, 586.

26. Nyquist, R. R. and Kagel, R. O. *Infrared Spectra of Inorganic Compounds: 3800-45 cm⁻¹*; Academic Press: New York, 1971.
27. Busca, G.; Centi, G.; Marchetti, L. and Trifiro, F. *Langmuir* **1986** 2, 568.
28. Wachs, I. E., *J. Catal.* **1990** 124, 570.
29. Klug, H. P.; Alexander, L. E. *Diffraction Procedures for Polycrystalline and Amorphous Materials*, 1st Ed., Wiley: New York, 1954.
30. Severin, K. G.; and Ledford, J. S., unpublished results.
31. Wachs, I. E.; Saleh, R. Y.; Chan, S. S. and Chersich, C. C.; *Appl. Catal.* **1985** 15, 339.
32. Iwaki, T.; Miura, M. *bull. Chem. Soc. Jpm.* **1971** 44, 1754.
33. Radecka, M.; Zakrzewska, K.; Czternatsek, H.; Stapinski, T. *Appl. Surf. Sci.* **1993** 65/66, 227.
34. So, H.; Pope, M. T. *Inorg. Chem.* **1972** 11, 1441.
35. Iwamoto, M.; Furukawa, J.; Matsudami, K.; Takenaka, T.; Kagawa, S. *J. Am. Chem. Soc.* **1983** 105, 3719.
36. Schraml-Marth, M.; Wokaun, A.; Baiker, A. *J. Catal.* **1990** 124, 86.
37. Flynn, C. M., and Pope, M. T. *J. Amer. Chem. Soc.* **1986** 92, 2715.
38. Sawatzky, G. A. and Post, D.; *Phys. Rev. B* **1979** 20(4), 1546.
39. Nickl, J.; Schlogl, R.; Baiker, A.; Knozinger, H. and Ertl, G.; *Catal. Lett.* **1989** 3, 379.

Chapter 3

Effects of Doping Levels on Vanadium Oxide/Titanium Oxide Thin Film Conductimetric Sensors

3.1 Introduction

The previous chapter discussed the effects of annealing temperature on the structure of sol-gel produced vanadium oxide/titanium oxide thin films. Continuing this two-part investigation of the influence vanadium has on the structure of titanium oxide thin films, we present here the effects of changing vanadium doping levels. Again, preparation involved the hydrolysis of metal alkoxides using excess valeric acid at room temperature. Data shows that the structure of the thin films could be changed by altering the vanadium doping level. XPS data show the dependence of the vanadium oxidation state and the V/Ti surface atomic ratio on bulk V concentration. No crystalline vanadium oxide was detected by XRD in any sample up through a 0.025 bulk V/Ti atomic ratio. Crystalline TiO_2 (anatase) was observed in all films, with the relative concentration and particle size of TiO_2 crystals showing a dependence on the vanadium loading. UV-Vis data also show that the amount of vanadium present in the film does not affect the TiO_2 band gap.

TiO_2 -based metal oxide sensors have been the focus of studies to evaluate their properties under various conditions including exposure to oxygen [1-5], humidity [6], and NO_x compounds [7]. Much evidence has shown that mixed metal oxides interact and provide different properties than that of the metal oxide alone [8-10]. The $\text{V}_2\text{O}_5/\text{TiO}_2$ system is widely used in industry because of its catalytic properties. These properties

include the reduction of nitric oxide in the presence of ammonia [11-13] and the oxidation of hydrocarbons [14,15]. The catalytic activity and selectivity has been found to be dependent on the amount of surface vanadium present. The optimal activity occurs when a monolayer of vanadium is formed [13]. The presence of excess vanadium results in the formation of crystalline V_2O_5 . However, a moderate amount of this oxide species does not significantly change catalytic activity, since crystalline V_2O_5 shows poor selectivity towards these analytes [16].

Using sol-gel chemistry, mixed metal oxides can be obtained from metal alkoxide precursors [17-19]. The alkoxide precursors undergo an inorganic polymerization reaction resulting in a metal oxide backbone. The mixing of alkoxide precursors allows homogeneous, multicomponent systems [20] leading to glasses at lowered temperatures. The rheological properties of the resulting materials can be utilized to produce materials through a wide variety of techniques [21-23]. It has been shown that the rate of the hydrolysis and condensation reactions can be controlled by the introduction of carboxylic acids [20,24]. Carboxylic acids affect the rates by complexing with the alkoxide precursor and slowing the condensation reaction [25]. Stable and uniform thin films that adhere well to quartz have been produced through the chemical modification of the alkoxide precursors with valeric acid [26,27].

The effects of vanadium loading on the properties of the mixed oxide have previously been studied [28-34]. It is widely accepted that vanadium 'wets' crystalline TiO_2 up to the point of a monolayer [34] and a mechanism for this wetting (or migration) has been proposed [35]. All systems previously studied have involved crystalline TiO_2 (primarily anatase) as a starting material combined with vanadium either by mechanical

methods or through wet impregnation. There has not been a reported study of the V/Ti system synthesized via sol-gel chemistry. A purpose of the present research was, therefore, to study how vanadium loading affects the structure of the resulting V_2O_5/TiO_2 system in materials prepared through sol-gel techniques.

Uniform vanadium oxide/titanium oxide thin films were prepared from vanadium triisopropoxide oxide, titanium (IV) isopropoxide and valeric acid. Films were prepared with varied doping levels of vanadium and characterized using a combination of surface and bulk methods. X-ray photoelectron spectroscopy (XPS) was used to provide information about the chemical species present in film surfaces and their relative concentrations. X-ray diffraction (XRD) provided information about the crystal structures in the films. Ultraviolet-visible spectroscopy (UV-Vis) was used to determine the coordination of the vanadium species present and determine the band gap of TiO_2 in each film.

3.2 Experimental

Materials. Valeric acid (99+%, Aldrich Chemical Co.), Titanium (IV) isopropoxide (97%, Aldrich Chemical Co.), and vanadium triisopropoxide oxide (Gelest Inc.) were used without further purification. Distilled, deionized water was used for all preparations.

Solution Preparation. Sols were prepared similarly to the method previously developed for titanium [36]. Since both metal precursors are easily hydrolyzed, solutions

were prepared in a glovebox under continuous N₂ purge. The vanadium loadings were varied to produce sols with V/Ti atomic ratios of 0.26, 0.53, 0.111, 0.176, and 0.250. Vanadium triisopropoxide was added to titanium (IV) isopropoxide followed by the addition of valeric acid and then water. The reactions were carried out at room temperature in capped vials. The metal:water:acid ratio was 1:1.5:9. The solutions were vigorously shaken with a vortex mixer following the addition of each reactant and were prepared in duplicate.

Film Preparation. The solutions were deposited on a quartz substrate and spun for a minimum of 5 minutes and air-dried overnight. Films were then annealed at 400°C for 24 hours in a tube furnace under the flow of dry air (100 cc/min, medical grade, AGA Gas). Film preparations from each solution were carried out in triplicate.

Reference films were prepared containing vanadium oxide or titanium oxide separately. The solutions and films were prepared in similar manner to those containing both vanadium and titanium. The film containing vanadium oxide was annealed at 500°C for 4 hours. The titanium oxide film was annealed at 600°C for 4 hours.

X-ray Photoelectron Spectroscopy (XPS) Films cast on quartz slides were analyzed with a VG Microtech spectrometer using a Clam2 hemispherical analyzer. Data were collected with a Mg anode operated at 15 kV and 20 mA (300W) and an analyzer pass energy of 50 eV. The core electron regions for four elements were scanned with each film: C 1s O 1s, Ti 2p_{3/2} and V 2p_{3/2}. Binding energy charge corrections for films containing Ti were made with reference to the Ti 2p_{3/2} peak (Ti 2p_{3/2} = 458.5 eV [37]). Corrections for reference films of V₂O₅ were made with reference to C 1s (284.6 eV).

The binding energies given have a precision of ± 0.1 eV. Quantitative measurements from XPS data were performed using the sensitivity factors determined previously [38]. For quantitative determination of the V $2p_{3/2}$ region, the contribution from the O 1s satellite was subtracted out from the area attributed to V $2p_{3/2}$. The V/Ti surface ratio was calculated from the core level features of each film. Curve fitting was performed using a 20% Lorentzian-Gaussian mix Voigt function [39].

X-ray Diffraction (XRD). All films were analyzed with a Rigaku XRD diffractometer using Cu K α radiation ($\lambda = 1.5418$ Å). The X-ray tube was operated at 45 kV and 100 mA. The diffractometer scanned at a rate of 0.07 deg/min (deg = 2θ). Divergence and scattering slits were both set at 1°. Background due to the quartz substrate has been subtracted from each of the patterns.

Ultraviolet-visible spectroscopy (UV-Vis). UV-Vis spectra was collected with a Unicam spectrometer. The incident beam was normal to the surface of the film using a blank quartz slide as a reference. Data were collected using Vision software in absorbance mode with a bandwidth of 2 nm and a data interval of 1 nm.

3.3 Results and Discussion

XRD. The XRD patterns for the various atomic ratios are presented in Figure 3.1. The only feature observed with XRD was due to TiO₂(anatase), thus the range presented is between 2θ values of 24.50 and 26.50. The formation of TiO₂(anatase) crystals from a completely amorphous TiO₂ film requires a temperature of at least 600°C [38]. However,

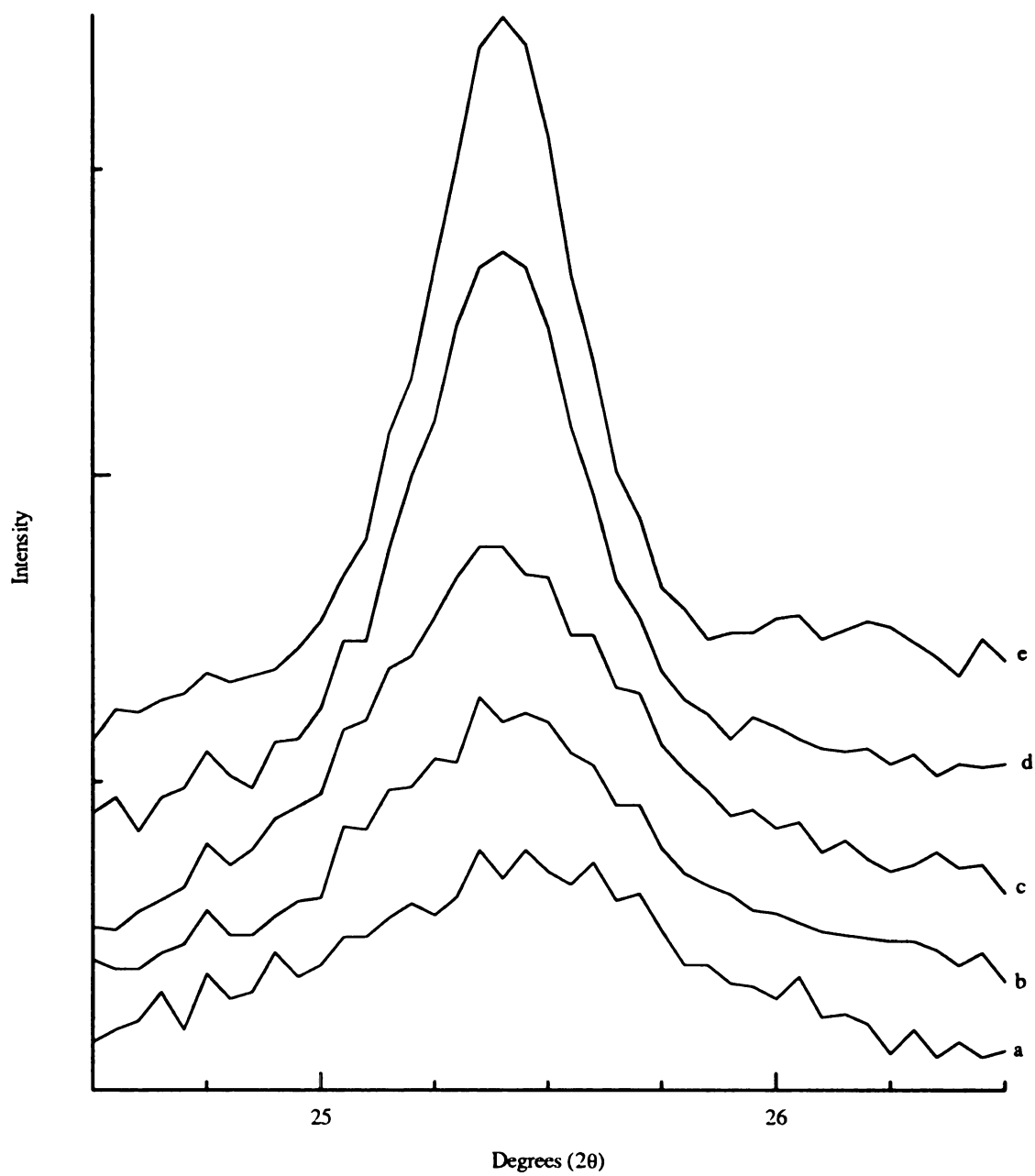


Figure 3.1. XRD diffraction patterns obtained for V/Ti atomic ratios of: (a) 0.026, (b) 0.053, (c) 0.111, (d) 0.176, (e) 0.250.

we have shown the presence of vanadium influences the crystallization of amorphous titanium at lower temperatures [40]. The broad feature appearing at the lowest loading indicates the presence of even small amounts of vanadium will initiate crystal formation of $\text{TiO}_2(\text{anatase})$. As the loading is increased, an increase in the relative intensity of the anatase peak is observed suggesting the increased presence of vanadium further promotes the formation of $\text{TiO}_2(\text{anatase})$. Vanadium crystals are not evident in the XRD patterns.

Along with the increased intensity of the $\text{TiO}_2(\text{anatase})$ diffraction pattern, narrowing of this feature's FWHM was also observed. A decrease in the linewidth of an XRD diffraction pattern is indicative of the formation of smaller particles [41]. Table 3.1 shows the particle sizes of $\text{TiO}_2(\text{anatase})$ that were calculated from FWHM values of XRD patterns using the Scherrer equation [41]. These calculations show an increase in the TiO_2 particle size as the vanadium loading increases. Calculations also suggest a minimum particle size of $\sim 120 \text{ \AA}$ could be obtained at 400°C through control of vanadium loading.

Table 3.1. Particle size of $\text{TiO}_2(\text{anatase})$ as determined through line broadening calculations of XRD diffraction patterns.

Bulk V/Ti Atomic Ratio	FWHM	Particle Size (\AA)
0.026	0.65	125
0.053	0.68	120
0.111	0.61	133
0.176	0.44	187
0.250	0.36	224

Bond et al. [33] observed XRD lines due to vanadium oxide for V/Ti mixed oxide catalysts containing a vanadium loading greater than 0.029 V/Ti atomic ratio. Saleh *et al.* [16] observed a trace amount of crystalline V_2O_5 in a catalyst with a 0.111 V/Ti atomic ratio. Our results indicate that the vanadium loading can be significantly increased beyond previously studied V/Ti systems without the formation of vanadium oxide crystals.

UV-Vis. For reference, Figure 3.2a contains UV-Vis data collected from an amorphous TiO_2 thin film containing anatase crystals. Confirmation of the presence of crystals in the film was obtained through XRD analysis of the film. The broad absorbance below 350 nm can be attributed to an electron transition from the valence to conduction band of TiO_2 [42]. Figure 3.2 also contains a spectrum from a film primarily composed of V_2O_5 (3.2b). The absorbances observed for a vanadium oxide film are the result of a charge transfer from vanadium to a terminal oxygen [10]. Schraml-Marth *et al.* [43] report tetrahedrally coordinated vanadium(V) shows a charge transfer transition in the 285-335 nm region while the charge transfer transition for octahedrally coordinated vanadium(V) occurs in the 400-500 nm region. The differences in the energies of the absorbances in our spectrum of vanadium oxide suggest differences in coordination of vanadium, where absorbances at 400 and 265 nm represent vanadium in its +5 oxidation state with octahedral and tetrahedral coordinations, respectively.

Figure 3.3 presents the UV-Vis spectra obtained from films with varied atomic ratios of V/Ti. The strong absorbance below 350 nm in all spectra can be attributed to TiO_2 . There is also a broad feature appearing in the TiO_2 anatase film in the higher wavelength region between 400 and 1000 nm. Tetrahedrally coordinated vanadium(V)

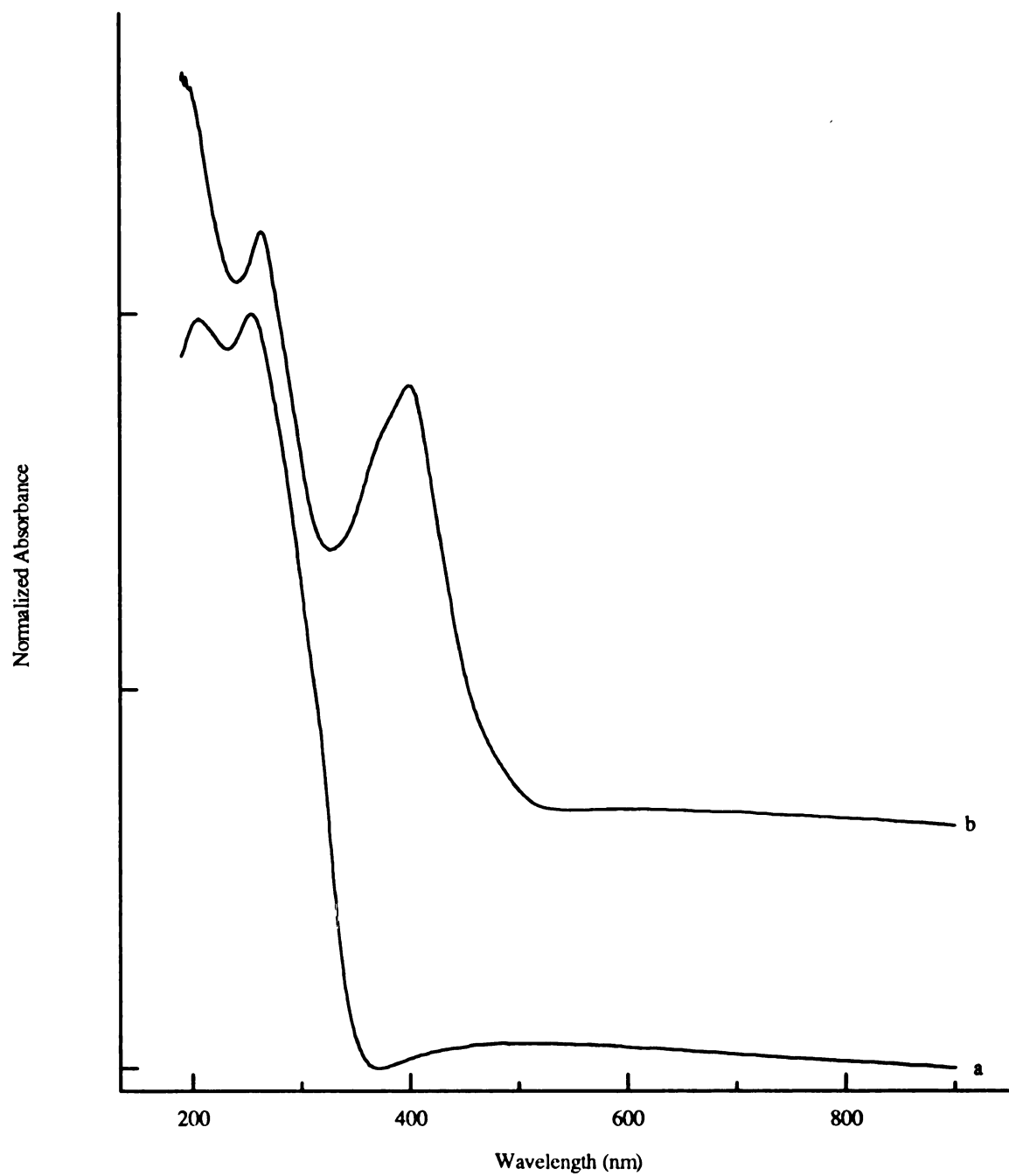


Figure 3.2. UV-Vis spectra for reference films containing (a) TiO₂(anatase) or (b) V₂O₅.

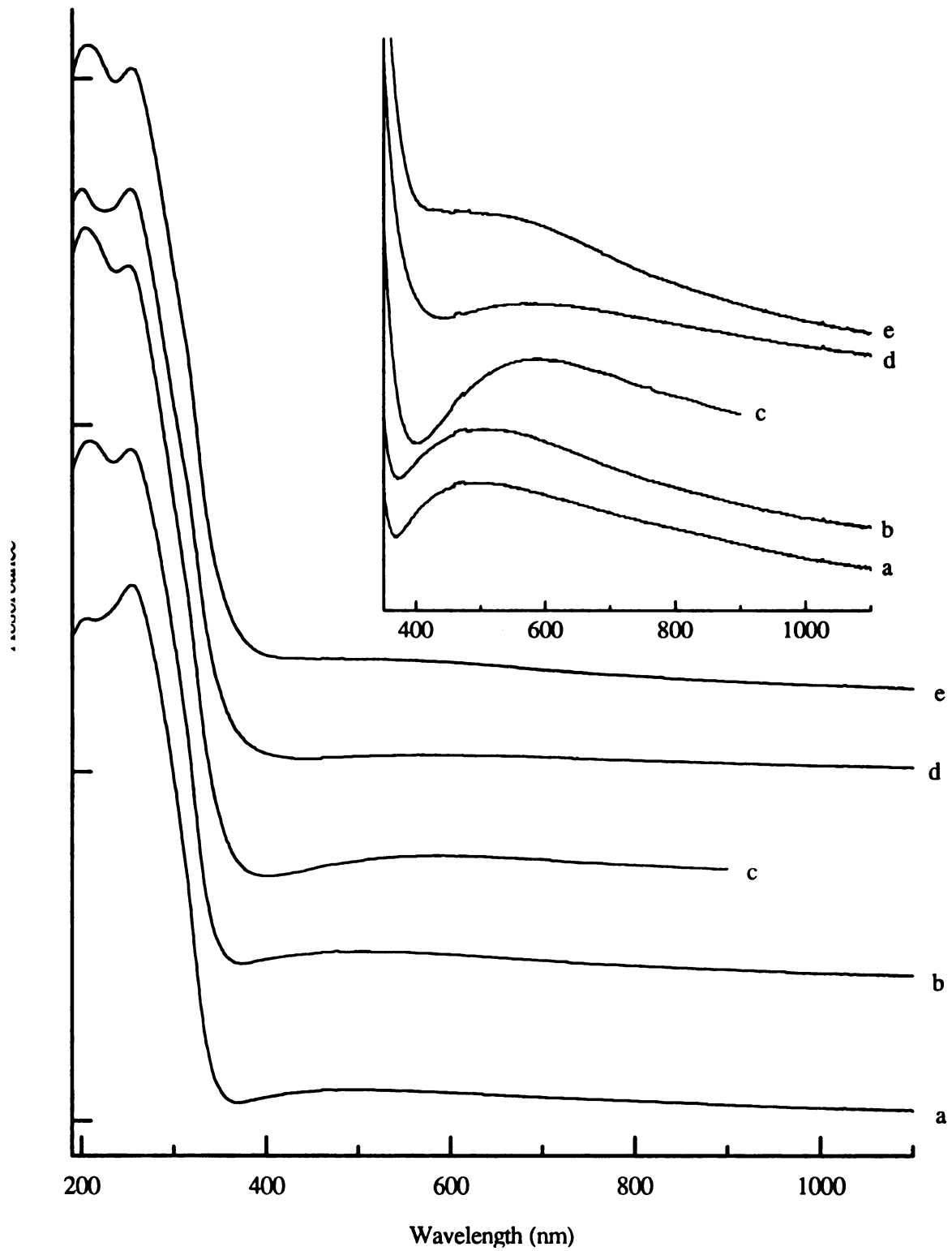


Figure 3.3. UV-Vis spectra for films containing V/Ti atomic ratios of (a) 0.026, (b) 0.053, (c) 0.111, (d) 0.176 and (e) 0.250.

absorbs ultraviolet radiation below 350 nm. The strong TiO_2 feature also absorbing in this region will not allow for this species to be differentiated in our spectra since the signal for the vanadium species will be much weaker. The feature above 400 nm shifts and becomes broader with the introduction of vanadium. There are two possibilities for vanadium ionic states that could contribute to this broad absorption feature. First, octahedrally coordinated V(V) will absorb between 400 and 500 nm and second, V(IV) in an octahedral environment will absorb between 770 and 625 nm. At the lowest atomic ratios, the vanadium ions remained in the +5 oxidation state, as evidenced by the increased absorbance between 400 and 500 nm. When the vanadium loading was increased, the absorbance near 500 nm began to shift to a higher wavelength. This shift can be attributed to an increased presence of V(IV) caused by the interaction of the vanadium species with anatase crystals of TiO_2 . When the vanadium loading is increased to 0.176 V/Ti, a shift back to lower wavelength is observed. This shift is attributed to an increased presence of vanadium that is fully oxidized to V^{5+} and is octahedrally coordinated. This trend continues for the film derived from a sol containing a 0.250 V/Ti atomic ratio.

Another interesting feature that comes from our studies of semiconducting materials that can be detected through UV-Vis spectroscopy is the band gap of TiO_2 . The band gap of TiO_2 can be measured from the tail at the high wavelength end of the UV-Vis absorbance. Accurate measurements of this tail have been discussed by Ibanez *et al.* [44]. The band gap was determined for the film containing TiO_2 (anatase) (Figure 3.2a) to be 3.57, slightly greater than the gap of 3.4 eV reported by Tang *et al.* for single crystal TiO_2 (anatase) [45]. The band gap values for films containing atomic ratios between 0.026

and 0.250 as well as the value representing a primarily anatase film are presented in Table 3.2. The reported values have a relative standard deviation <1%. The TiO₂ band gap remains constant as the V/Ti atomic ratio is increased, suggesting that the band gap is not affected by the amount of vanadium present in our materials. Gautron et al. [46] observed a significant reduction of the TiO₂ band gap to to near 2 eV when VO₂ was introduced into TiO₂.

Table 3.2. Measured Band gaps measured for V/Ti films. A film containing TiO₂(anatase) crystals is included for reference.

Bulk V/Ti Atomic Ratio	Band gap (eV)
TiO ₂	3.6
0.026	3.6
0.053	3.6
0.111	3.5
0.176	3.5
0.250	3.5

XPS. The shifting of V 2p_{3/2} binding energy as a function of loading has been studied by various groups (see, for example, ref. [32]). An increased binding energy of the V 2p_{3/2} feature is observed as a result of the increased vanadium content in the film (Figure 3.4). When the V/Ti ratio is 0.026, a binding energy of 516.0 eV is observed. According to previously published data on vanadium oxides [47], a feature occurring in this region can be assigned to the vanadium ion primarily in its 4+ oxidation state. Since free vanadium ions are easily reduced under vacuum, it is conceivable that the vanadia species on the film surface is reduced prior to analysis with XPS (which occurred at a pressure of ~10⁻⁹ torr). The binding energy of V 2p_{3/2} increases by 0.5 eV when the V/Ti

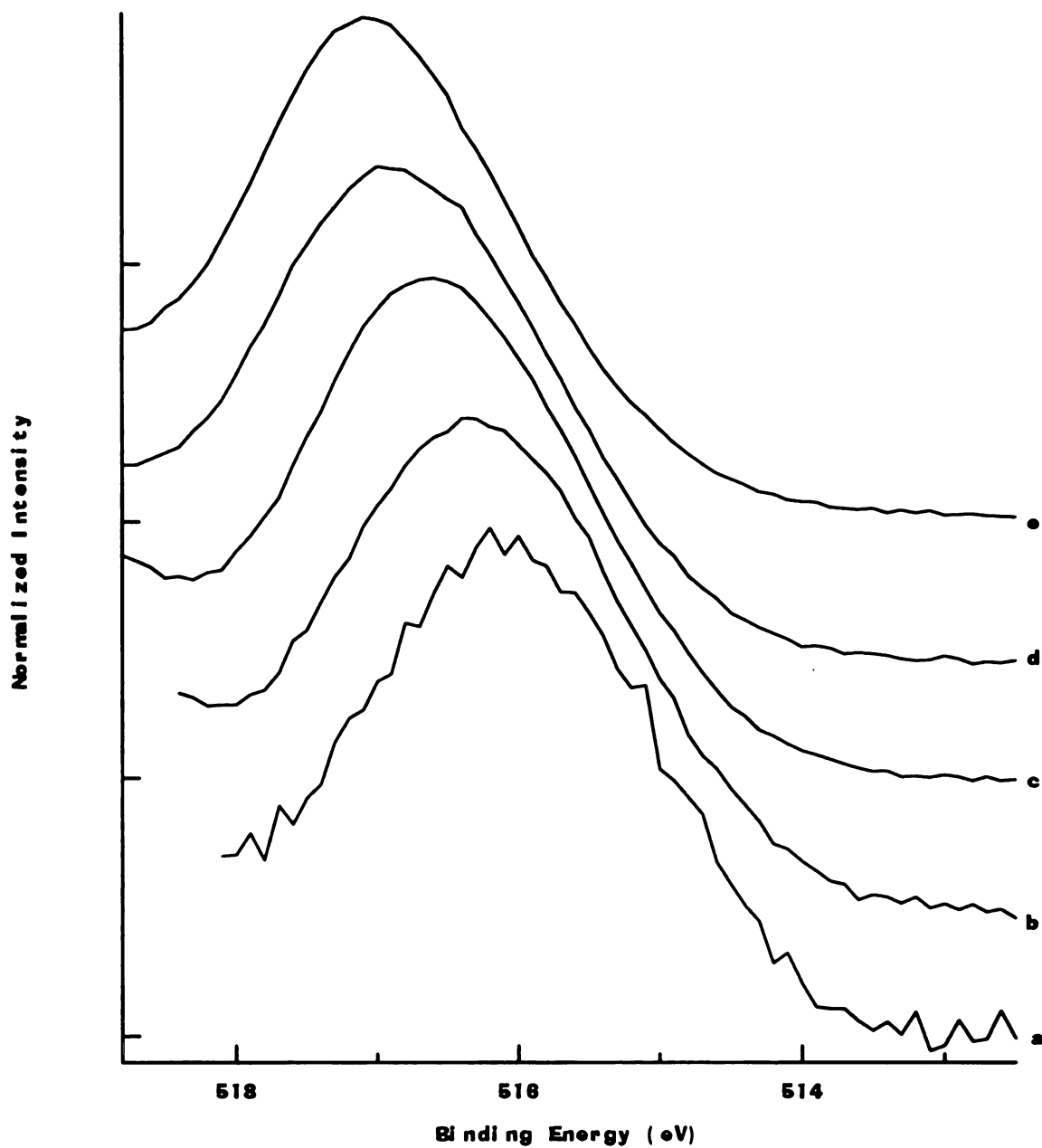


Figure 3.4. XPS results showing the effect of vanadium loading on the feature due to $V2p_{3/2}$. Films were derived from sols with (a) 0.026 (b) 0.053, (c) 0.111, (d) 0.176, and (e) 0.250 V/Ti atomic ratios.

atomic ratio is increased to 0.053. This feature can be attributed to the presence of both V^{4+} and V^{5+} in the surface of the film [47]. The V $2p_{3/2}$ binding energy increases more gradually when the mole ratio is increased further. The resulting shift to a higher binding energy (516.9 eV for 0.250 V/Ti atomic ratio) suggests the amount of V^{5+} increases in the surface of the film with increased loading. The surfaces of films with the highest vanadium content contain primarily V^{5+} .

The O 1s core level remained unchanged when the loading of vanadium was altered (Table 3.3), assuring that the V $2p_{3/2}$ peak shift was not an artifact of the binding energy correction. For all samples, the oxygen peak contained a strong feature due to the backbone species centered at 529.8 eV with a shoulder appearing at 531.6 eV due to hydroxyl groups bonded to TiO_2 on the surface of the film.

Table 3.3. XPS data for films derived from sols containing between 2.5 and 20% V.

V/Ti Atomic Ratio	Surface* V/Ti Atomic Ratio	BE O 1s	BE V $2p_{3/2}$
0.026	0.023	529.8	516.0
0.053	0.079	529.8	516.5
0.111	0.189	529.8	516.7
0.176	0.310	529.8	516.8
0.250	0.395	529.8	516.9

*Determined from V $2p_{3/2}$ / Ti $2p_{3/2}$ intensity ratios.

When altering the V/Ti mole ratio of the alkoxide precursors, the surface composition of the resulting metal oxide thin film changes as shown in Figure 3.5. At the lowest vanadium loading, the surface atomic ratio in the film is close to (within experimental error) the bulk atomic ratio. However, when the bulk ratio was increased

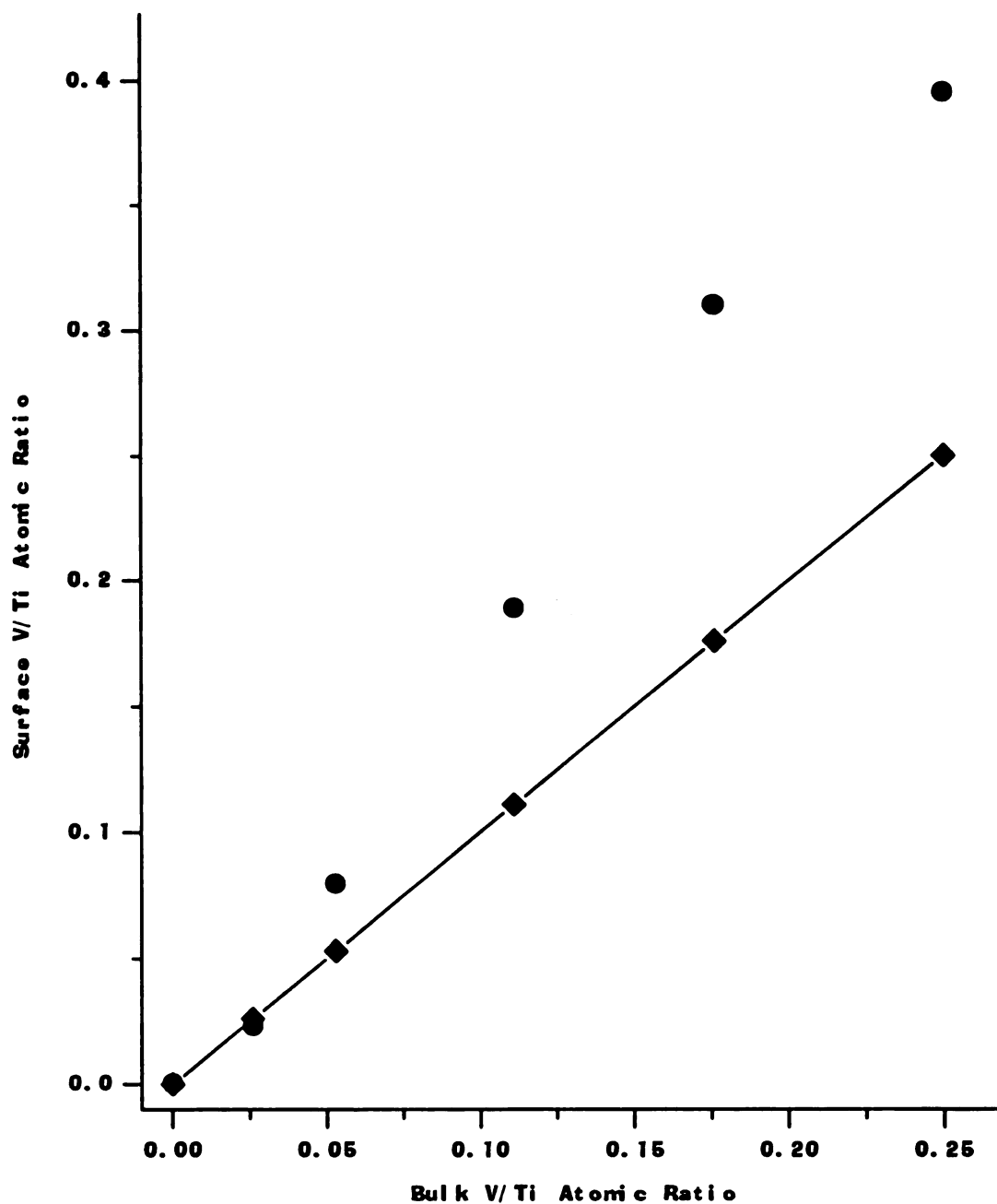


Figure 3.5. Comparison of surface and bulk V/Ti atomic ratios. Experimental data represented by circles. Squares represent a plot for equal bulk and surface ratios.

above 0.025, the V/Ti surface ratio was higher than the bulk V/Ti ratio. XRD data presented earlier showed the increased concentration of TiO_2 (anatase) crystals as a result of increased vanadium loading with the particle size also increasing with vanadium loading. A higher surface ratio than the bulk ratio is attributed to the V species in the V/Ti mixture 'spreading' across the TiO_2 crystals. The increased presence of TiO_2 crystals along with the increased particle size of these crystals provides a mechanism for the observed migration of the vanadium species to the film's surface. The migration of vanadium is consistent with earlier results for catalysts derived through wet impregnation of the vanadium species on a TiO_2 (anatase) support [48]. The V/Ti surface ratio increases consistently up to the film containing a 0.111 bulk ratio. At higher vanadium content, however, the rate of increase of the surface ratio shows non-linearity. Stranick *et al.* [49] showed that this decreasing non-linearity of the surface ratio vs. bulk ratio plot indicates a poorly dispersed dopant on the support, so our non-linear relation between bulk and surface ratios suggests a poorly dispersed vanadium phase. This poorly dispersed phase is attributed to the formation of crystalline V_2O_5 . The fact that peaks are not observed in XRD diffraction patterns indicates the V_2O_5 particles are smaller than 0.3 nm (the detection limit for XRD [50]).

3.4 Conclusions

The use of sol-gel chemistry has allowed the formation of TiO_2 (anatase) at low loadings, an increased amount of anatase crystals with increased vanadium content, and

further increased vanadium loading to the point suggesting the formation of crystalline vanadium oxide. Materials in the current study have shown a change in the observed monolayer coverage compared to materials obtained through traditional catalyst preparation techniques.

We have shown in the previous chapters that temperature affects both the surface and bulk structure of sol-gel derived vanadium oxide/titanium oxide thin films [40]. The present study has shown the level of bulk vanadium in V/Ti thin films also affects the film's surface and bulk structures. Both vanadium and titanium crystal structures change as the bulk atomic ratio changed. While vanadium loading mainly affects the particle size of the TiO_2 (anatase) crystals, the vanadium species present in the film changed from completely amorphous at low loadings to amorphous and crystalline at higher loadings. XPS data suggests the vanadium ions present in the surface of the film are also influenced by the bulk vanadium concentration.

The surface atomic ratio of V/Ti was observed by XPS as the bulk ratio was changed. Two conclusions can be made from the change in surface V/Ti ratio: First, the non-linearity of the bulk vs. surface atomic ratios indicates a crystalline vanadium species was formed although not detected through XRD. Second, the trend of the increasing surface V/Ti ratio being greater than the increased vanadium doping suggests the vanadia species spreads over the TiO_2 crystals, consistent with observations made by Haber et al. [35]. Although the band gap of our films differs from that of crystalline TiO_2 , the gap was not affected by the doping level of vanadium in the films.

Vanadium loading can be used to control the surface and bulk phases of both transition metals in a V/Ti oxide system. The use of sol-gel technology to prepare these mixed metal-oxide thin films has allowed us to change the surface structure and morphology from that previously defined with technical catalysts.

3.5 List of References

1. Kirner, U.; Schierbaum, K. D.; Göpel, W. Leibold, B.; Nicoloso, N.; Weppner, W.; Fischer, D.; Chu, W. F. *Sens. Act.* **1990** *B1*, 103.
2. Göpel, W.; Kirner, U.; Wiemhöfer, H. D.; Rocker, G. *Solid State Ionic* **1988** *28-30*, 1423.
3. Xu, Y.; Yao, K.; Zhou, X.; Quanxi, C. *Sens. Act. B* **1993** *13-14*, 492.
4. Hasegawa, S.; Sasaki, Y.; Matsuhara, S. *Sens. Act. B* **1993** *13-14*, 509.
5. Wu, M. T.; Yao, X.; Yuan, Z. H.; Sun, H. T.; Wu, W. C.; Chen, H. Xu, G. Y. *Sens. Act. B* **1993** *13-14*, 491.
6. Nenov, T.; Yordanov, S.; *Sens. Act. B*, **1992** *8*, 117.
7. Boccuzzi, F. Guglielminotti, E. *Sens. Act. B*, **1994** *21*, 27.
8. Stencel, J. M.; Makovsky, L. E.; Sardus, T. A.; de Vries, J.; Thomas, R.; Mouljin, J. A. *J. Catal.* **1984**, *90*, 314.
9. Soled, S.; Murrel, L. L.; Wachs, I. E.; Mc Vicker, G. B.; Sherman, L. G.; Chan, S. S.; Despenziere, N. C.; Baker, R. T. K. in *Solid State Chemistry in Catalysis*; Brasselli, R. K., Brazkil, J. F., Eds.; American Chemical Society: Washington, DC, 1985; p.165.
10. Wachs, I. E.; Saleh, R. Y.; Chan, S. S.; Chersich, C. C. *Appl. Catal.* **1985**, *15*, 339.
11. Tufano, V. and Turco, M. *Appl. Catal.* **B2** (1993) 9.
12. Turco, M.; Lisi, L.; Pirone, R.; *Appl. Catal.* **B2** (1994) 133.
13. Went, G. T.; Leu, L.-J., Rosin, R. R.; and Bell, A. T.; *J. Catal.* **134** (1992) 492.
14. Rao, C. N. R.; Raju, A. R.; and Vijayamohan, K., Gas-sensor Materials in *New Materials*, S. K. Joshi, C. N. R. Rao, R. Rsruta and S. Nagakura (eds.), New Delhi, India, 1992, pp. 1-37.
15. Martin, C.; Rives, V.; Sanchez-Escribano, V.; Busca, G.; Lorenselli, V.; and Ramis, G., *Surf. Sci.* **251/252** (1991) 825.
16. Saleh, R. Y.; Wachs, I. E.; Chan, S. S.; Chersich, C. C. *J. Catal.* **1986**, *98*, 102.
17. Yoldas, B. E. *J. Non-Cryst. Solids* **38, 39** (1980) 81.
18. Wark, T. A.; Gulliver, E. A.; Jones, L. C.; Hampden-Smith, M. J.; Rheingold, A. L.; Huffman, J. C. in *Better Ceramics Through Chemistry IV*, Zelinsky, B. J. J.; Brinker, C. J.; Clark, D. E.; Ulrich, D. R., Eds.; Mater. Res. Soc. Proc. 180; Pittsburg, PA (1990) 61.
19. Wellbrock, U.; Beier, W.; Frischat, G. H. *J. Non-Cryst. Solids* **147,148** (1992) 350.
20. Livage, J.; Henry, M.; Sanchez, C. *Prog. Solid State Chem.* **18** (1989) 259.
21. Sakka, S.; Kamiya, K.; *J. Non-Cryst. Solids* **1982** *48*, 31.
22. Dislich, H.; Hinz, P. *J. Non-Cryst. Solids* **1982** *48*, 11. .
23. Clark, D. E. in *Science of Ceramic Chemical Processing*, Hench, L. L. and Ulrich, D. R. Eds., Wiley: New York, 1986, p.237.
24. Brinker, C. J.; Scherer, G. *sol-Gel Science*; Academic Press: San Diego, 1990.
25. Sanchez, C.; Livage, J. *New J. Chem.* **1989** *18*, 513.

26. Gagliardi, C. D.; Berglund, K. A. in *Better Processing Science of Advanced Ceramics*, Askay, K. A.; McVay G. L.; Ulrich, D.R., Eds.; Mater. Res. Soc. Proc. 180; Pittsburg, PA (1986) 127. b)
27. Gagliardi, C. D.; Berglund, K. A. in *Better Processing Science of Advanced Ceramics*, Askay, K. A.; McVay G.L.; Ulrich, D. R., Eds.; Mater. Res. Soc. Proc. 180; Pittsburg, PA (1986) 127.
28. Wachs, I. E.; Saleh, R. Y.; Chan, S. S.; Chersich, C. *chemtech* **1985**, 756.
29. Went, G. T.; Leu, L. J.; Bell, A. T. *J. Catal.* **1992**, 134, 479.
30. Inomata, M.; Mori, K.; Miyamoto, A.; Murakami, Y. *J. Phys. Chem.* **1983**, 87, 761.
31. Lietti, L.; Forzatti, P.; Ramis, G.; Busca, G.; Bregani, F. *Appl. Catal. B* **1993**, 3, 13.
32. Nickl, J.; Schlögl, R.; Baiker, A.; Knözinger, H. and Ertl, G.; *Catal. Lett.*, **3** (1989) 379.
33. Bond, G. C.; Sarákány, A. J.; Parfitt, G. D. *J. Catal.* **1979**, 57, 476.
34. Wachs, I. E.; Jehng, J. M.; Hardcastle, F. D. *Solid State Ionics* **1989** 32/33, 904.
35. Haber, J.; Mqchej, T.; Servicka E. M.; Wachs, I. E. *Catal. Ltr.* **1995**, 32, 101.
36. Severin, K. G.; Ledford, J. S.; Torgerson, B. A.; Berglund, K. A. *Chem. Mater.* **1994** 6, 890.
37. Wagner, C. D.; Riggs, M. W.; Davis, L. E.; Moulder, J.; Muilenberg, G. E. *Handbook of X-Ray and Photoelectron Spectroscopy*, Physical Electronics Industries, Eden Prairie, MN, 1979.
38. Severin, K. G.; Ledford, J. S. *unpublished results*.
39. Software provided by Dr. Andrew Proctor, University of Pittsburgh, Pittsburgh, PA.
40. Hoffman, L. W.; Ledford, J. S. *manuscript in preparation*.
41. Klug, H. P.; Leroy, E. A. *X-Ray Diffraction Procedures for Polycrystalline and Amorphous Materials* Wiley-Interscience: New York, 1974.
42. Iwaki, T.; Miura, M. *bull. Chem. Soc. Jpm.* **1971** 44, 1754.
43. Schraml-Marth, M.; Wokaun, A.; Baiker, A. *J. Catal.* **1990** 124, 86.
44. Ibanez, J. G.; Solorza, O.; Gomez del-Campo, E. *J. Chem. Ed.* **1991** 68(10), 872.
45. Tang, H.; Lévy, G.; Berger, H.; Schmid, P. E. *Phys. Rev. B* **1995** 52(11), 7771.
46. Gautron, J.; Lemasson, P.; Poumellec, B.; Marucco, J-F. *Solar Energy Mat.* **1983**, 9, 101.
47. Sawatzky, G. A. and Post, D.; *Phys. Rev. B* **1979** 20, 1546.
48. Kihenski, J.; Baiker, A.; Glinski, M.; Dollenmeier, P.; Wokaun, A. *J. Catal.* **1986** 101, 1.
49. Stranick, M. A.; Houlalla, M.; Hercules, D. M. *J. Catal.* **1987** 103, 151.
50. Niemantsverdriet, J. W. *Spectroscopy in Catalysis* VCH: New York, 1993.

Chapter 4

Future Work

In the previous two chapters I have shown that the chemical state and structure of the surface species in V/Ti thin films can be controlled through loadings and annealing temperatures. By increasing the temperature, the surface V/Ti ratio increases. This increase in surface ratio is attributed to the 'wetting' of the vanadium species on the TiO₂ crystals as they are formed - with larger crystals forming at higher temperatures. The amount of vanadium present in the bulk also affects the surface V/Ti ratio. Again, larger TiO₂ crystals are formed with increased bulk V/Ti ratio, allowing the vanadium species to spread on these crystals.

It is desirable to correlate the information derived from the present studies with the activity of these thin films to develop a more complete understanding of the V/Ti metal oxide thin film conductimetric sensor. As outlined below, the device to conduct sensor measurements has already been developed. The next step will be to determine the system to be used for initial sensor measurements. Through catalysis studies, the active site of the V/Ti system in the oxidation of hydrocarbons is attributed to the reducibility of the surface vanadium species [1]. Correlating this information with results from chapter 2 pertaining to the surface V/Ti ratio, the best system to use for initial sensor measurements would be a thin film containing 0.111 bulk V/Ti atomic ratio prepared at 600°C. This film contains a high surface V/Ti ratio with no indication of crystalline vanadium formed and is therefore

presumed to show high surface activity and selectivity towards surface reactions with reducing analyte gases such as hydrocarbons.

4.1 Sensor measurements.

Since we are interested in a systematic investigation of the structure-reactivity correlations of V/Ti metal oxide sensor materials, a system must be developed to carry out the sensor measurements. In parallel with the studies described previously, we have developed a device to make conductivity measurements using the semiconducting properties of our metal oxide thin films. The preparation of the thin film on an alumina substrate has been adapted from earlier work published by Göpel and co-workers [2], and is shown schematically in Figure 4.1. The oxide substrate we chose to use was polished alumina. The most commonly used electrodes are gold; however, the adhesion of the oxide surface to the gold breaks down at high temperatures. Platinum, with the use of a titanium adhesion layer, however, has been shown to withstand high temperatures [2]. When titanium is deposited, a titanium oxide layer approximately 10-20 Å thick will form on the alumina substrate. Further deposition results in the formation of a Ti metal layer on the TiO_2 . Platinum can then be deposited on the Ti metal layer with good adhesion. Our method to deposit the thin metal films involved physical vapor deposition of Ti and Pt. A tungsten boat containing the particular metal was resistively heated by applying a current to the melting point of that metal. The deposited Ti layer was approximately 100 Å thick while the Pt layer for the electrodes was approximately 500-800 Å thick. The Pt heater

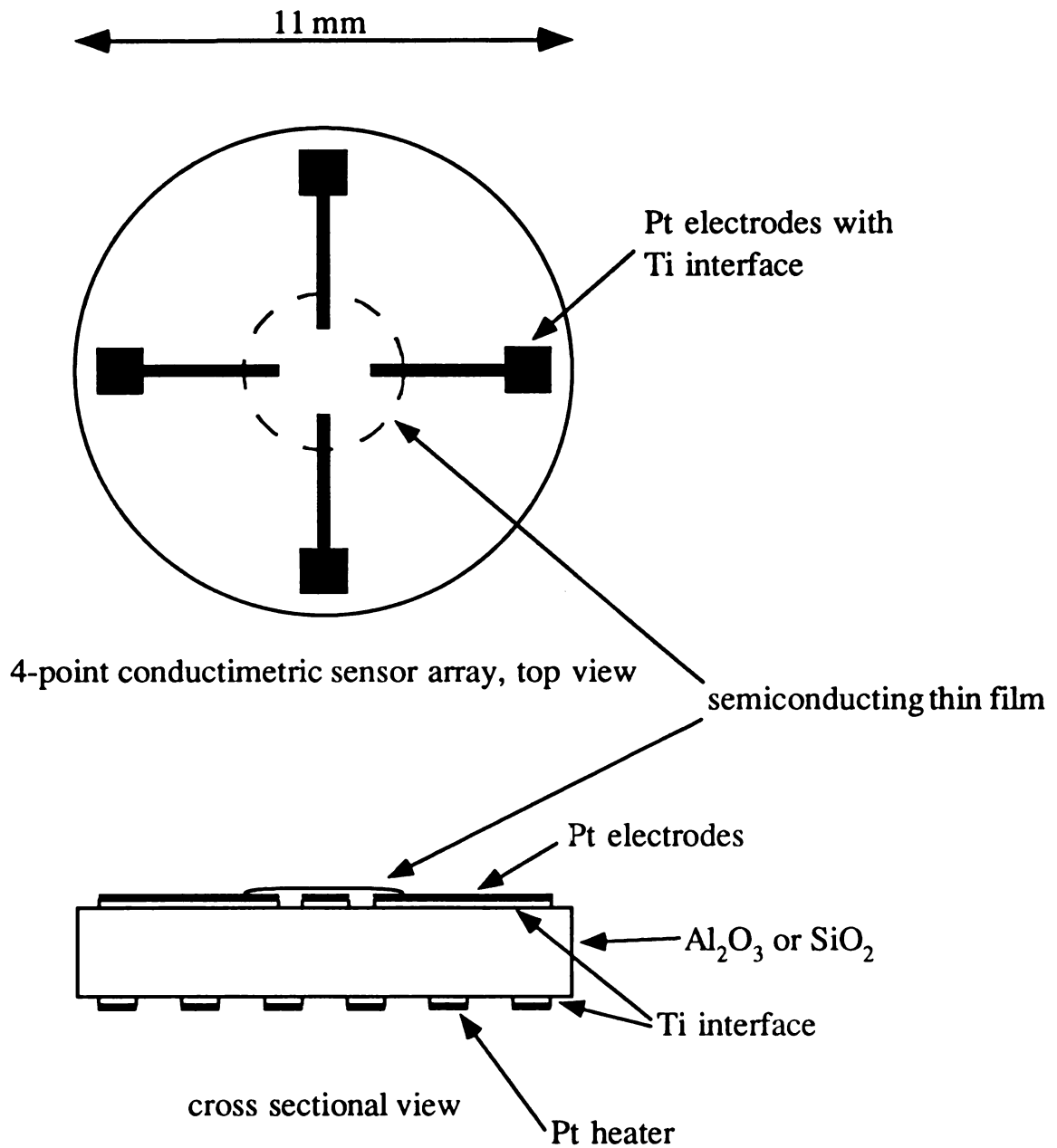


Figure 4.1. Schematic of sensor array.

also used a Ti adhesion layer with the platinum approximately 2-3 μm thick. Gold wires were bonded to the platinum surfaces to serve as electrical contacts. A schematic diagram of the cell used to make the sensor measurements is shown in figure 4.2. A gas of interest may be delivered to the cell from cylinders using mass flow controllers. Control and data acquisition are handled through a PC that is interfaced with the flow controllers and electronics of the cell.

A known current will be applied across two opposite electrodes on the sensing substrate with a resistance measured across the other two. When a particular analyte gas is passed over the surface of the thin film, reaction of this analyte gas with the surface will change the conductance of the surface (as outlined in chapter 1), thus changing the resistance of the thin film. The sensor response to a particular analyte can then be characterized assuming a linear relationship between concentration of the analyte gas and resistance of the film.

4.2 Oxidation reactions.

Initial experiments would involve a study of the effect of reducing gases such as CO or CH₄ on sensor response. As stated in the introduction, reducing gases are expected to react with adsorbed oxygen on the surface thereby changing the conductance of the film's surface. We have shown that many different surface phases can be obtained in our thin films via vanadium loading and/or annealing temperature. However, the ease in reduction of our surface V by analyte gases is not known. The oxidation of hydrocarbons

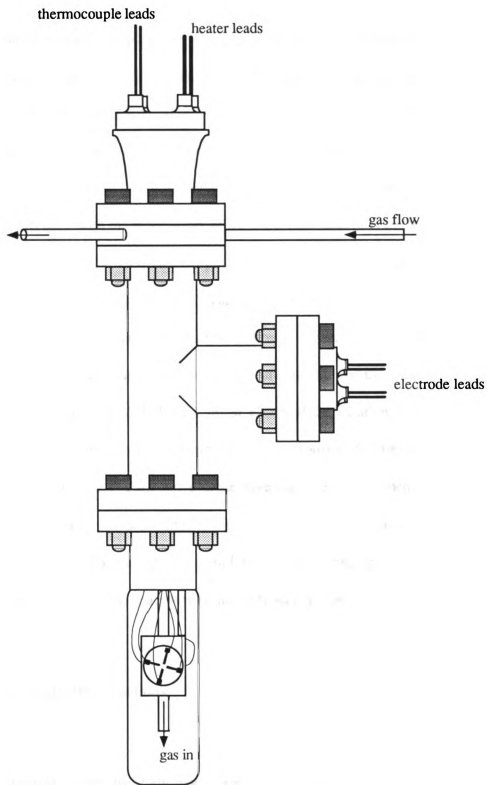


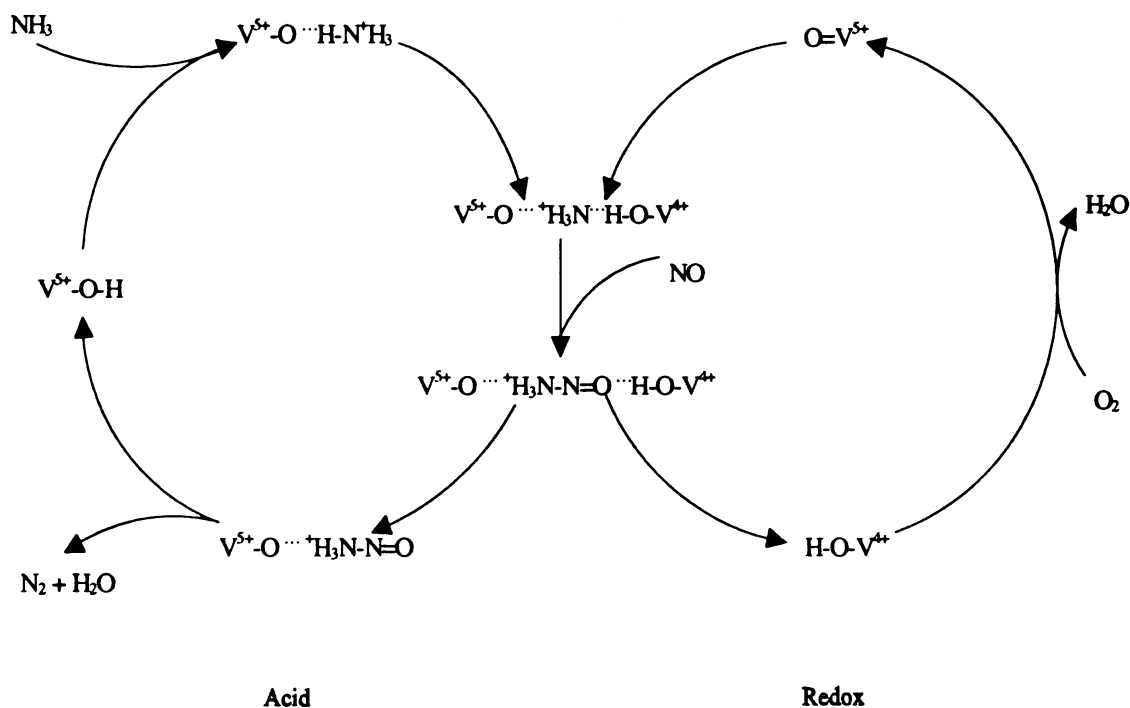
Figure 4.2. Cell used to make sensor measurements.

over vanadia catalysts supported by titanium oxide has been studied extensively [1,3-7]. In one particular study, the partial oxidation of methanol by vanadia species supported on TiO_2 , Deo and Wachs [1] suggest that the activity of the surface vanadium oxide phase is independent of loading when the vanadium oxide content is kept below monolayer coverage. These authors concluded that the surface reactivity of vanadium oxide/titanium oxide is correlated with the reducibility of the supported vanadium oxide. Gasior *et al.* [3] studied the effect of the TiO_2 support phase (anatase or rutile) on the selective oxidation of o-xylene to phthalic anhydride. The results of their study led to the following conclusions: anatase-containing samples 1) show a higher activity and selectivity in the oxidation of o-xylene, 2) have a lower degree of reduction of the vanadia species during the catalytic oxidation, and 3) have a lower observed dehydration/dehydrogenation ratio than rutile-containing samples. The surface states responsible for the catalytic oxidation of hydrocarbons over vanadia/titanium dioxide have been well established. However, our use of sol-gel technology has produced V/Ti thin films with surface structures different from those used in previous studies. It would therefore be interesting to study the surface phases responsible for sensor activity resulting from exposure to various reducing gases.

4.3 Reduction reactions.

Another interesting study would involve the response measurement of the surface of a V/Ti film in the presence of various NO_x compounds. We have shown the films to be stable up through an annealing temperature of 600°C. This would allow for a study of

automobile exhaust to determine the amounts of NO_x compounds via conductimetric sensing if the sensor response to NO_x has been developed. The use of vanadia/titania catalysts for the reduction of NO_x compounds in the presence of ammonia has also received much attention [8-18]. Early studies by Inomata *et al.* [8] have shown that the surface oxygen species $\text{V}=\text{O}$ speeds up the $\text{NO}-\text{NH}_3$ reaction. By studying the activity of the reduction of NO over vanadia on varied supports, these authors have shown the $\text{NO}-\text{NH}_3$ reaction to be structure insensitive. Thus, a higher amount of surface activity can be attained through a higher concentration of $\text{V}=\text{O}$ species. Topsøe *et al.* [12] have recently reported the catalytic activity of NO_x reduction over vanadia/titania catalysts is due to two different reactions occurring on the surface, denoted as acid or redox, as reported below:



The adsorption of ammonia occurs at the Brønsted acid sites or V^{5+} -OH. After a partial transfer of the acidic proton, NO can react with the intermediate to produce the released products, N_2 and H_2O . Oxidative regeneration of the reduced vanadium species in V^{4+} -OH to fully oxidized $V=O$ species completes the cycle.

In view with information presented in the last two sections, the field of chemical sensors utilizing properties of the vanadia/titania system provides many opportunities for research. The control of oxidation states, crystallinity, and surface structures of both vanadium and titanium (leading to a change in the concentration of $V=O$) provides an interesting starting point for the study of conductimetric sensor responses of vanadia/titania thin films with respect to various analyte gases.

4.4 List of References

- 1 Deo, G; Wachs, I. E. *J. Catal.* **1994**, *146*, 323.
- 2 Schierbaum, K.D.; Vaihinger, S.; Göpel, W.; Van Den Vlekkert, H.H., Kloeck, B. De Rooij, F. *Sens. Act.*, **1990**, *B1*, 171.
- 3 Gasior, M.; Gasior I.; Grzybowska, B, *Appl. Catal.* **1984**, *10*, 87.
4. Rusiecka, M.; Grzybowska; Gasior, M.; B, *Appl. Catal.* **1984**, *10*, 101.
- 5 Busca, G.; Elmi, A.; Forzatti, P. *J. Phys. Chem.* **1987**, *91*, 5263.
- 6 Wachs, I. E.; Saleh, R. Y.; Chan, S. S.; Chersich, A. C. *Appl. Catal.* **1985**, *15*, 339.
7. Deo, G; Wachs, I. E. *J. Catal.* **1994**, *146*, 335.
- 8 Inomata, M.; Miyamoto, A.; Ui, T.; Kobayashi, K.; Murakami, Y. *Ind. Eng. Chem. Prod. Res. Dev.* **1982**, *21*, 424.
- 9 Wong, W.C.; Nobe, K. *Ind. Eng. Chem. Prod. Res. Dev.* **1984**, *23*, 564.
- 10 Baiker, A.; Dollenmeier, P.; Glinski, M.; Reller, A. *Appl. Catal.* **1987**, *35*, 351.
- 11 Went, G.T.; Leu, L.-J.; Rosin, R.R.; Bell, A.T. *J. Catal.* **1992**, *134*, 492.
- 12 Topsøe, N.-Y.; Topsøe, H.; Dumesic, J.A. *J. Catal.* **1995**, *151*, 226.
13. Topsøe, N.-Y.; Dumesic, J.A.; Topsøe, H. *J. Catal.* **1995**, *151*, 241.
- 14 Handy, B.E.; Maciejewski, M.; Baiker, A. *J. Catal.* **1992**, *134*, 75.
15. Schneider, M.; Scharf, U.; Wokaun, A.; Baiker, A. *J. Catal.* **1994**, *150*, 284.
16. Ciambelli, P.; Bagnasco, G.; Lisi, L.; Turco, M.; Chiarello, G.; Musci, M.; Notaro, M.; Robba, D.; Ghetti, P. *Appl. Catal. B* **1992**, *1*, 61.
17. Tufano, V.; Turco, M. *Appl. Catal. B* **1993**, *2*, 9.
- 18 Turco, M.; Lisi, L.; Pirone, R.; Ciambelli, P.. *Appl. Catal. B* **1994**, *3*, 133.

